ABSTRACT

SIKKA, SIRAT. Studying Protein-Protein Interactions using Dynamic Light Scattering and Taylor Dispersion Analysis. (Under the direction of Dr. John van Zanten).

Protein-protein interactions are a major factor in maintaining protein colloidal stability. Colloidal stability influences critical attributes such as protein solubility, aggregation propensity, protein dispersion viscosity, and protein-surface interactions thus impacting biologic product function. In the production of biopharmaceuticals, immense effort is employed to determine the most propitious salt and buffer conditions to develop a drug product that is efficacious and safe for patient administration.

In this study, dynamic light scattering (DLS) was utilized to characterize protein-protein interactions. Interaction parameter, k_D, was determined from the protein collective diffusion coefficient protein concentration dependence as measured by DLS for bovine serum albumin (BSA) dispersed in various solvents. The initially repulsive interactions were found to decrease and attractive interactions ultimately were observed as salt concentration increased. The use of k_D as a quantitative tool to predict intermolecular interactions was confirmed. A comparatively rarely used method for protein sizing, Taylor dispersion analysis (TDA) was investigated as to its applicability for characterizing protein-protein interactions as a faster alternative to DLS. The obtained diffusion coefficients were compared to those found from DLS and found to agree qualitatively but not quantitatively.

Studying Protein-Protein Interactions using Dynamic Light Scattering and Taylor Dispersion Analysis

by
Sirat Sikka

A thesis submitted to the Graduate Faculty of
North Carolina State University
in partial fulfillment of the
requirements for the degree of
Master of Science

Biomanufacturing

Raleigh, North Carolina

2015

APPROVED BY:

Dr. John van Zanten
Committee Chair

Dr. Gary Gilleskie

Dr. Nathaniel Hentz

DEDICATION

I dedicate this thesis to my parents and my brother for their unconditional love and support.

BIOGRAPHY

Sirat Sikka was born in Hyderabad, India Oct 12 1989. She completed her schooling from National Public School, Bangalore and with the advent of Biotechnology in India the interdisciplinary nature of the subject motivated her to take that up as her Bachelor's program.

Four years of Bachelor's at Sree Nidhi Institute of Science and Technology (affiliated to Jawaharlal Nehru Technological University, Hyderabad, India) gave her the opportunity to explore many areas of biotechnology and learn skills related to bioprocess engineering, plant tissue culture, bioinformatics amongst other subjects. During this period Sirat interned at Dr. Reddy's Laboratories and Osmania University. Following graduation she joined Osmania University where she worked at the Department of Environmental Toxicology under the guidance of Dr. Hema Prasad, Head of Department.

The foregoing experiences increased her interest in the Biopharma industry and the Biomanufacturing program at BTEC coincided perfectly with her goals. She began her master's degree studies at BTEC, NC State in January 2013. During the program Sirat focused on the Downstream Track. She worked as a Teaching Assistant to Dr. John van Zanten for the graduate and undergraduate courses in Biological Processing Science from August 2013 to Dec 2014. Sirat was also involved with NCSU-ISPE student chapter as the Public Relations Director from Jan 2014 to Dec 2014. Her summer internship was at Novartis Holly Springs, NC where she worked in Global Technical Downstream Development. After completing her master's degree studies, she aspires to work in process development in Biopharma and maybe latter pursue her PhD in a related field.

ACKNOWLEDGMENTS

This has been a very brief, yet power packed, high voltage and a tense journey, and at its culmination there are many wonderful people to whom I wish to extend my heartfelt appreciation.

Foremost, I am enormously grateful to Dr. John van Zanten for giving me the opportunity to work with him and be showered with all his mentorship, focus, support, understanding and guidance through the last two years. It was a pleasure to assist him with undergraduate and graduate courses at BTEC.

I am thankful to Dr. Gary Gilleskie and Dr. Nathaniel Hentz for their support through course work and research.

My work would not have fructified without the support from Dr. Micheal Flickinger. I am grateful for his guidance through my master's program.

I want to thank Christopher Smith for all his help and advice through the program. He has always been very kind. I would also like to thank Winnell Newman and Ray Annover.

I want to thank all BTEC faculty and staff with a special mention to Dr. Jennifer Ruiz, Dr. Amith Naik, and Jessica Weaver for their guidance with research activities at BTEC annex, as well as Brain Mosley and Rebecca Kitchener for helping me with all the work at the analytical lab and relevant training sessions.

My sincere thanks to Jennifer Sasser, Michele Ray, Ketan Shah and Eric Sarfaraz for their help with all the resources required for my work, BTAs LaShonda Herndon, Maria Kostyukovsky and John Taylor for helping me with managing various activities around the labs.

I would like to thank Drs. Samuil Amin, Wei Qi, Stacy Kenyon, Kevin Mattison and Mark Pothecary from *Malvern Instruments* for their help and cooperation.

I am also grateful to Julia Deuel and Dr. Stephanie Cope from *Wyatt Technology* for their training and guidance.

I am thankful to Mark Wilson, Francesco Berlanda-Scorza, Chris Dadd and Lauren Crumpler from Novartis. My internship there helped me be productive with my research.

During the summer of 2013 I worked at BTEC along with Andrew Ray and want to thank him. I would like to thank Jennifer Lu as well.

I want to thank my friends Nishanth, Kishore, Priyanka, Sriram, Sharath, Nikhil, Sameer, Shamik, Raghul, Tanuja, Kiran, Srujana and Anirudh.

Lastly I am thankful to my parents and my brother for their high spirited emotional support and encouragement throughout the entire journey of this study.

TABLE OF CONTENTS

LIST OF TABLES

LIST OF FIGURES

LIST OF ABBREVIATIONS

Amm S	Ammonium sulphate
BSA	Bovine Serum Albumin
B_{22}	Second Osmotic Virial Coefficient
c	Concentration
DLS	Dynamic Light Scattering
D	Diffusion Coefficient
D_o	Diffusion Coefficient at Infinite Dilution
EDL	Electrical Double Layer
FFF	Field Flow Fractionation
k_D	Interaction Parameter
LS	Light Scattering
M	Molarity
MALS	Multiangle Light Scattering
NaCl	Sodium Chloride
NaBr	Sodium Bromide
pI	Isoelectric Point
PBS	Phosphate Buffer Saline
Rh	Hydrodynamic Radius
RI	Refractive Index
SLS	Static Light Scattering
TDA	Taylor Dispersion Analysis

Chapter 1

Introduction

Proteins have been developed and successfully commercialized as therapeutics for several decades, targeting a broad spectrum of diseases. The first protein based treatment was introduced in 1923 when insulin extracted from bovine and porcine pancreas was marketed as Iltein for treating diabetes mellitus Type I and II. Although this was a turning point for diabetes care, there were drawbacks such as organism availability and disease transmission from other organisms [1]. Subsequent biologic products included blood components, polyclonal antibodies from human plasma (1940s) and blood enzymes such as the antihemophilic factor VIII. The discovery and introduction of recombinant DNA technology in the 1970s provided a means for producing human therapeutic proteins in other organisms without the limitations associated with protein extraction from other species. Genes could then be manipulated to synthesize a desired protein and the market for protein therapeutics has exhibited significant growth since. These processes, however, produce multiple impurities and biotherapeutics themselves are susceptible to degradation and other unfavorable modifications. In response to these observations and in an attempt to overcome associated challenges processes have been developed to achieve desired protein therapeutic critical quality attributes. In order to deliver efficacious, safe and superior quality protein therapeutics, industry utilizes techniques to thoroughly characterize product structure and function.

Proteins have several advantages over small molecule drugs. Proteins are highly specific, thereby exhibiting fewer side effects, and more effective and some being more compatible with the human body than chemically synthesized drugs [2]. The challenges lie in the

production process. The process depends on the type of protein, its synthesis pathway (intracellular or extracellular) and how sensitive it is to degradation and changes in processing conditions. For example, some intracellular production processes lead to the formation of inclusion bodies and refolding therapeutic proteins from these large aggregates is a huge challenge as that can potentially lead to the loss of function if misfolded and loss of protein product making the purification process inefficient.

If production buffers are improperly chosen such that protein molecules exhibit attractive interactions for one another, potential aggregation may pose hindrance to processes such as filtration by clogging membranes, lead to an increase in viscosity or yield several problems during administration such as impact syringeability or cause adverse immune responses in patients. All these factors need to be taken into consideration when developing a biopharmaceutical manufacturing process.

Protein stability is a major concern during manufacturing and also storage. Proteins are susceptible to environmental factors and changes can cause either denaturation and/or aggregation. Naturally occurring human proteins have evolved to function at 37°C, near neutral pH and ~ 150 mM ionic strength. Proteins can respond to the very slight changes, if any, that occur *in vivo* and are still able to maintain their structure and function. However, during production proteins encounter environmental conditions that do not match the *in vivo* conditions wherein they have evolved. Several characterization methods for interrogating protein structure and aggregation state are available and employed. While a catastrophically compromised environmental condition, such as one readily leading to precipitation or formation of large aggregates, can be easily rejected by visual appearance, biophysical characterization is required to delineate the suitability of alternative environmental conditions. Large effort and time is expended by formulation scientists on developing the most suitable conditions for final drug product stability.

In order to understand environmental influence on proteins it is important to review some basic principles regarding their structure, stabilities – conformational and colloidal - and molecular level protein-protein interactions.

1.1 Protein Structure

Protein structure is very complex with the intricate folding of polypeptide chains determined by the properties of different amino acid residues. Figure 1.1 elucidates the levels of protein structure. The amino acid sequence is denoted the primary structure. Hydrogen bond formation and weak van der Waal's interactions give rise to secondary structures, denoted as alpha-helices or beta-sheets, depending on the structural organization of their constituent amino acid residues. The former conformation exhibits a helical backbone whereas the latter has polypeptide chains lying adjacent to one another and binding laterally via hydrogen bonds between the carbonyl oxygen and the amino hydrogen atoms. These strands maybe either parallel, where the N terminus of the strands is at the same end, or anti-parallel [3].

The folding and turning of these structures as a result of water-induced forces, weak van der Waal's forces, ionic bonds involving negatively and positively charged amino acids and disulfide bonds leads to formation the tertiary structure – the three-dimensional, spatial organization. Finally two or more of such polypeptide chains may associate to form a multi-subunit complex. In this case, the protein is said to exhibit quaternary structure.

Although the presence of aqueous solvent results in the protein core being made up of essentially all nonpolar residues, a significant fraction of nonpolar amino acid residues reside at the protein surface owing to their close proximity to polar residues in the primary structure. The water-induced forces that drive this structural organization is typically denoted the hydrophobic effect [3]. The protein surface exhibits a nonuniform distribution of hydrophobic and charged patches – both anionic and cationic.

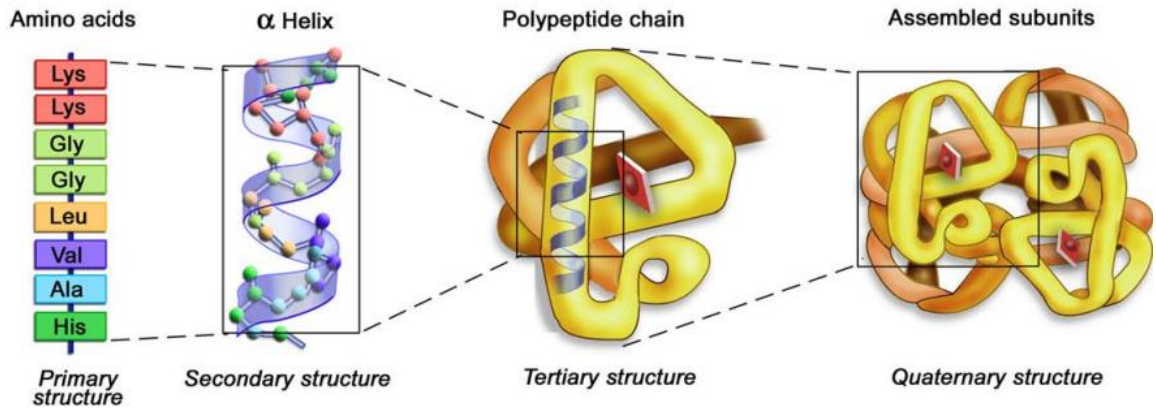

Figure 1.1 Levels of protein structure *[4]*.

Intramolecular interactions, or thermodynamics, are responsible for maintaining globular protein structure and stability [5] . The final conformation is only weakly stabilized – the free energy change upon unfolding is on the order of 5-20 kcal/mol. Because of these relatively low folding energies, protein conformation is very dependent on environmental conditions such as temperature, pH and solvent composition. An understanding of protein structure is important for studying and analyzing the protein-protein interactions, as the protein structural conformation and surface composition/topology play a crucial role in these biophysical processes.

1.2 Protein-Protein Interactions and Stability

There are two important protein stabilities to be considered - conformational and colloidal stability. Conformational stability refers to native protein structure maintenance. As noted previously, conformational stability is very sensitive to environmental conditions. Proteins *in vivo* are oftentimes protected by chaperons and very stable environmental conditions – neither of which is the case for therapeutic proteins during the manufacturing process.

Therapeutic proteins typically experience varying environmental conditions during manufacture, storage and formulation. As such, these processes greatly impact the ***intra***molecular forces that stabilize the protein conformation and affect the product form and function.

Our focus here is on colloidal stability or resistance to aggregation. Colloidal stability results from a balance between ***inter***molecular repulsive and attractive forces. Formulation efforts are focused on enhancing the former form of interactions such that the protein is maintained in its monomeric native form and aggregation is avoided. Essentially this is simply the physical science of interactions between charged particles in solutions of varying ionic strength/composition and/or pH. Just as in the case of conformational stability, colloidal stability is very sensitive to environmental conditions.

Although the protein surface exhibits charged and hydrophobic patches, the net protein charge can be considered as a starting point for colloidal stability. The protein net charge in solution changes with the buffer pH and can be either positive or negative depending on the protein isoelectric point (pI). The pI is defined as the pH at which the protein has zero *net* charge. This is a condition to avoid as the protein is least soluble when the pH is close to its isoelectric point. The relationship between protein charge and solution pH is shown in Figure 1.2.

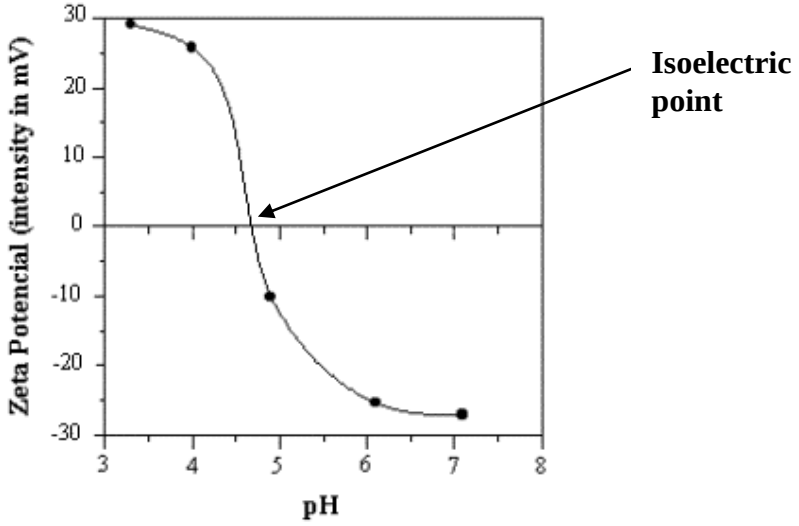

Figure 1.2 pH dependence of protein zeta potential *[6]*.

Protein-protein interactions are controlled by several phenomena – the electrical double layer, osmotic repulsion, attractive dispersion forces, hydration-water induced forces and finite size effects (hard sphere interactions). The first contribution results from the ion cloud (electrical double layer) that surrounds all charged particles in electrolyte solutions. The second contributing factor takes into consideration intermolecular osmotic and electrostatic repulsion and attractive forces such as weak van der Waal's forces. The hydration forces are very hard to account for and typically neglected although the past few years have seen some attempts to account for these contributions. The so-called hard sphere interaction, relating to finite size effects, notes that two proteins cannot occupy the same space. Since these interactions exhibit different length scales, the overall protein-protein interaction potential depends on the protein separation distance. The overall picture is that of a short-ranged (less than the molecular diameter) attractive potential.

1.3 Formulation

Instabilities such as conformational changes, aggregation and precipitation in protein pharmaceuticals are some of the major challenges met by continuous process improvements and parallel analytical testing of product quality [7]. There is an increasing awareness of stability issues that can arise during processing because of the labile nature of biologics and tremendous effort is focused on identifying optimum solvent conditions [8]. Changes in protein free energy are affected by temperature, pH and solvent composition making buffer selection a very crucial step in downstream processing and formulation of protein therapeutics [9]. The set of activities related to overcome the potential instability of the drug is referred to as *formulation development* [10]. A successful formulation development effort has four stages: preformulation, stabilization of the active substance in bulk form, formulation in the designated dosage forms and fill-finish aseptic manufacturing activities associated with the latter [10]. The major difficulty faced by a formulation group is selecting the right formulation components such as buffer, salts, sugars, amino acids, preservatives, viscosity modifiers, surfactants, *etc*. These components typically modify protein-protein interactions in order to achieve formulation goals and are very temperature and pH sensitive.

1.4 Testing Stability Indicating Factors

Several challenges are faced in maintaining protein stability during and after production. Proper formulation conditions maintain the protein therapeutic in a stable and efficacious form making the drug safe for patient administration. Adverse effects of improper formulation as negative impacts have been observed in clinical trials and following product introduction to the market [10]. In order to prevent the aforesaid, and thus determine best final formulation conditions significant effort is placed in developing and carrying out various preformulation studies that take into account the physico-chemical phenomena impacting product stability. Protein unfolding and aggregation assays are considered under

different stress conditions to give a range of conditions that would be most suitable [11]. Changes in conditions outside the optimum range can lead to protein damage that will cause function loss. Some protein instabilities can result from unfavorable protein-protein interactions under different conditions during drug development.

Typical biophysical methods for assessing conformational stability include differential scanning calorimetry, intrinsic and extrinsic fluorescence, circular dichroism and Raman spectroscopy. These methods are typically used to select several candidates for final formulation conditions. Industry is now more closely focusing on colloidal stability to evaluate these potential formulation conditions in more detail, as it is believed that maximizing both conformational and colloidal stability will yield superior pharmaceutical products. Potential robust, high throughput methods are of great interest. Light scattering is an example of such a technique that is non-invasive, non-destructive and is well suited for the determination of protein oligomers, a major product impurity. Static light scattering (SLS) is well known to provide the most direct access to the protein-protein interactions that underlie protein colloidal stability by determination of the osmotic second virial coefficient [12]. The time-averaged intensity also yields the molecular weight and root mean square radius. However, SLS is a difficult and slow characterization method to implement. Dynamic light scattering (DLS), on the other hand, is based on the fluctuations of the scattered light intensity. It is more robust and amenable to high throughput methodology (approximately 100 samples/day per instrument or even greater with the latest plate readers), but does not provide direct access to the thermodynamically relevant protein-protein interaction parameters. Therefore, current work is focused on understanding how DLS can provide insight into the relevant colloidal stability parameters analogous to that imparted by SLS measurements. DLS typically requires one to consider five or more protein solution concentrations in order to assess the colloidal stability parameter. The collective diffusion coefficient at each concentration is determined to ultimately provide insight into protein-protein interactions.

The potential to assess such information from studying a single protein concentration via another experimental technique would be of great interest as that would minimize time and resources spent. With the foregoing objective in mind, here we have begun to consider the use of Taylor dispersion analysis as an alternative to access such interaction information. It is important to study protein-protein interactions in great depth as they have a direct impact on the product and such analysis would help process and formulation development eventually yielding a product that is stable and hence safe for the patient.

The objective of this study is to assess colloidal stability by measuring the concentration dependence of the protein collective diffusion coefficient via dynamic light scattering, with protein-protein interactions being parameterized via the interaction parameter k_D, and comparing diffusion coefficient values measured using Taylor dispersion analysis (TDA). These comparisons were performed to assess the suitability of using TDA to carry out protein diffusion coefficient measurements as a function of protein concentration. Long-term goals at BTEC include developing a single measurement TDA method for determining the interaction parameter instead of analyzing a series of protein solution concentrations, as is currently done with DLS, and pioneering efforts with TDA. Bovine serum albumin (BSA) was chosen as a model protein for the studies. BSA or serum albumin derived from cow, is extensively used as a model protein in research. It has a total of 607 amino acids and a molecular weight of approximately 67 kDa (Figure 1.3) [13]. The isoelectric point is 4.7 [14]. Here, a BSA concentration series was formed in various buffers and the samples are characterized by both DLS and TDA in order to assess the concentration dependent collective diffusion coefficient in each case.

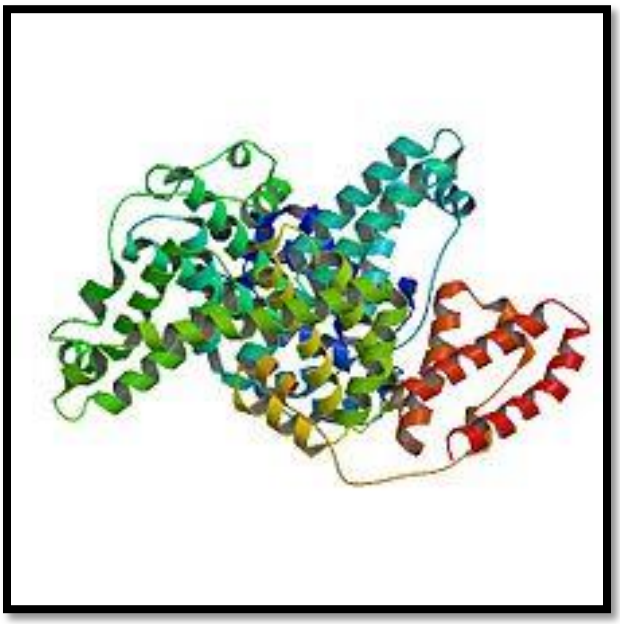

Figure 1.3 Crystal structure of Bovine Serum Albumin (BSA) *[13]*.

Chapter 2

Background

The complex nature of protein therapeutics has always posed difficulties for biologic production. As noted previously, conformational and colloidal stability must be maintained throughout manufacture, storage, formulation and fill/finish. Formulation requires one to determine the critical quality attributes, develop an efficient design of experiment approach for determining the best formulation candidates and ultimately testing their safety and efficacy in clinical trials. In addition to the stability issues other attributes may be of concern as well. For instance, if prefilled syringes are going to be the delivery mode protein dispersion viscosity will become an important parameter to consider as well. Ultimately conditions must be identified to ensure these goals are met and that a product with sufficient shelf life can be introduced to the market.

In what follows, some important protein biophysical chemistry will be reviewed, in particular, protein aggregation and protein-protein interactions. A brief discussion of protein-protein interaction characterization approaches will be presented as well. Finally, specific ion effects and the Hofmeister series are briefly considered.

2.1 Protein Aggregation

Protein aggregation is a complex self-assembly process mitigated by changes in environmental conditions such as pH, temperature and buffer composition. Irreversible aggregates or reversible self-associations lacking interprotein covalent bonds can exist. Figure 2.1 illustrates the aggregation process as described by *Amin S.et al* [15].

For instance, monomeric proteins could partially unfold and weakly associate with denatured molecules to form reversible aggregates. Since native state unfolding exposes the hydrophobic core thereby promoting self-association, conformational stability is of paramount importance. Recently researchers have acknowledged the potential importance of the native self-association pathway to protein aggregate formation. Maximizing native protein dispersion colloidal stability minimizes this pathway.

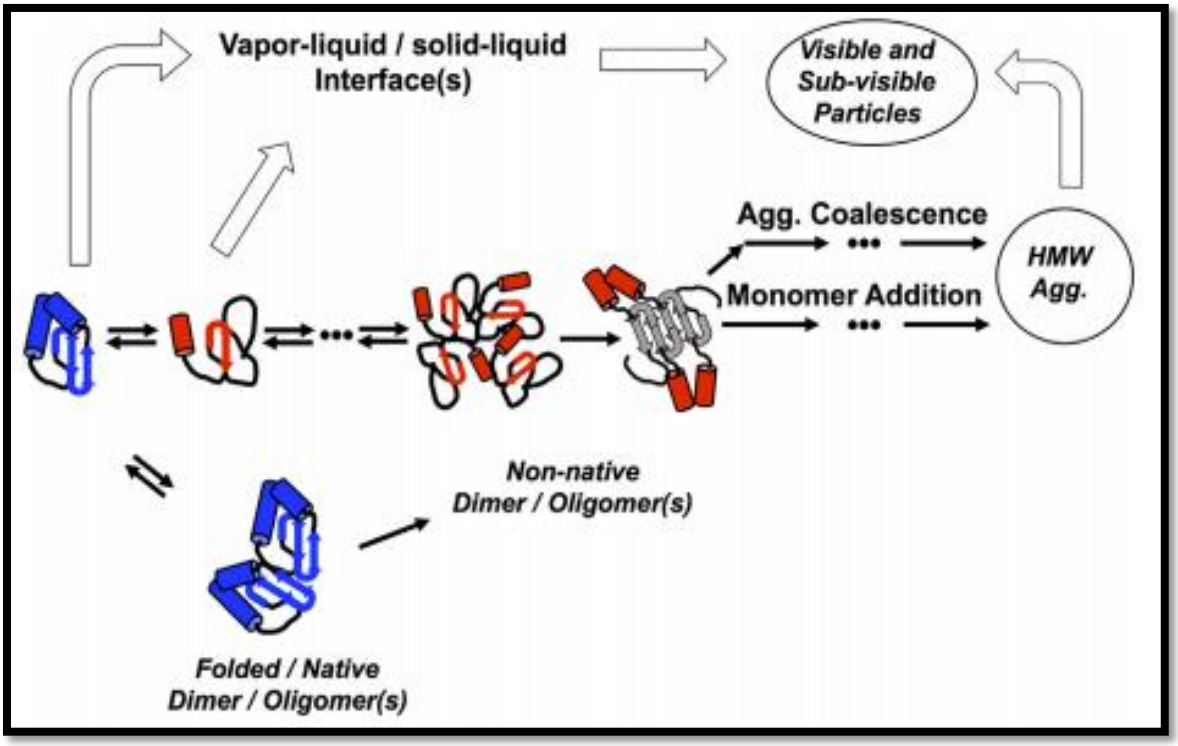

Figure 2.1 Irreversible and reversible aggregate formation *[15]*.

Protein aggregation is of great interest in biopharmaceutical manufacturing and also human physiology as many diseases are a result of protein aggregation [16] [17]. In protein therapeutic manufacturing protein aggregation hinders downstream operations and ultimately may lead to deleterious patient outcomes.

For example, during filtration processes the presence of precipitates or large aggregates increases process time due to membrane fouling requiring frequent filter module replacement leading to an increase in resource costs. Product aggregation can also result in reduced recovery during chromatography steps for purification or polishing. Thus, major efforts are dedicated to developing processes which produce minimal amounts of undesired oligomers. Solvent condition and protein concentration changes can influence protein aggregation, viscosity and liquid formulation physical stability (*i.e.* susceptibility to phase separation) [18]. Formulation scientists seek solvent combinations maximizing conformational and colloidal stability.

2.2 Protein-Protein Interactions

2.2.1 Interactions between Charged Particles

The *Derjaguin, Landau, Verwey and Overbeek* (DLVO) theory of interparticle interaction is the classic approach for explaining colloidal stability. This approach is based on a balance between repulsive electrostatic interactions and attractive van der Waal's forces with colloidal stability requiring the dominance of the former. Applications include predicting colloidal stability in numerous industrial processes such as liquid-liquid extraction, alkaline flooding operations, hydrocarbon flotation, oil droplet stability in emulsions, *etc.* [19]. Although the DLVO theory has been successfully utilized numerous times, numerous examples where it has failed exist (*Israelachvili et al.*) [20] [21] . The DLVO theory only considers ion charge and also assumes that ions are point charges thereby neglecting ion size

effects as well as non-Coulombic electrostatic interactions between charged particles and ions.

The origin of the repulsive electrostatic interactions lies in the ion cloud surrounding all charged particles dispersed in electrolyte solutions. As a first approximation proteins are assumed to be uniformly charged spheres. Ions of opposing charge to the sphere charge (counterions) are attracted to particle surface and are accompanied by their coions of opposite charge. This cloud or 'layer' of ions is denoted the electrical double layer (EDL). These electromagnetic forces are in competition with the omnipresent thermal forces. The balance between these forces ultimately establishes the length scale within which ions are closely associated with the charged sphere. This length scale is known as the Debye length, κ^{-1}, and it determines the distance over which repulsive interactions are important.

The Debye length thickness is a function of particle surface charge and polarizability and ion properties such as charge, polarizability and size. Repulsive particle-particle interactions arise from the fact that the EDLs on two closely approaching particles want to maintain their structure as is and therefore resist interpenetration. The EDL associated with a protein in solution is shown in Figure 2.2 [22].

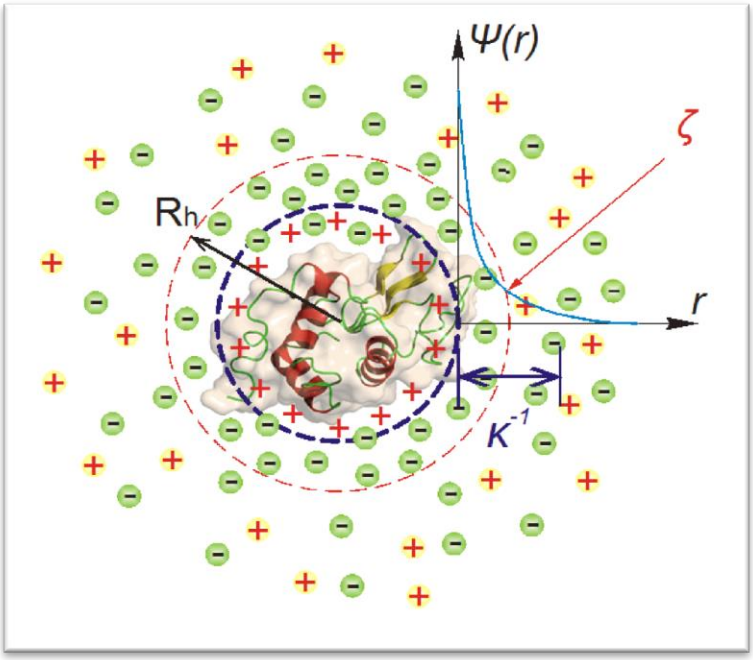

Figure 2.2 Schematic illustrating electrical double layer: R_h - Hydrodynamic radius, Ψ(r) electrostatic potential, κ^{-1} Debye length, ζ – Zeta potential , r- distance between molecules *[22]*.

Attractive interactions arise from dispersion forces sometimes also denoted as van der Waal's forces. The balance between these competing forces is illustrated in Figure 2.3 [23]. The potential barrier to aggregation is determined by the properties of the EDL or Debye length. DLVO theory, which only accounts for ion charge, indicates that the EDL will decrease with increasing ion valency and concentration. Recent theoretical approaches have accounted for complexities presented when one accounts for ion charge, polarizability and size [24].

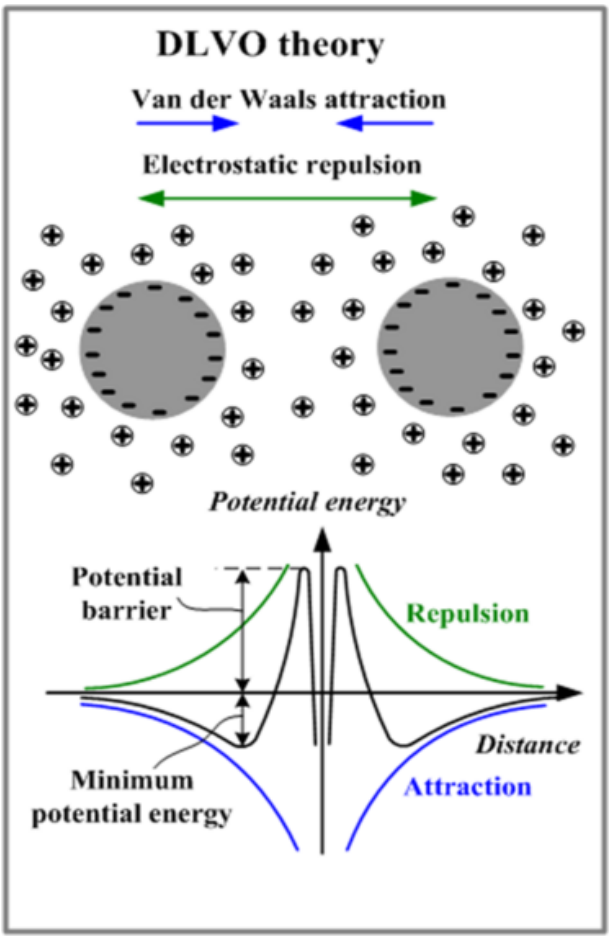

Figure 2.3 Schematic illustrating the DLVO theory *[23]*.

It should be noted that standard colloidal interaction theories assume colloidal particles are uniformly charged dielectric hard spheres. In reality, proteins are non-spherical in shape and exhibit surface roughness whose length scale is comparable to the overall protein size. In addition, protein surface composition is very heterogeneous in that one can observe charged (both positive and negative) and hydrophobic patches randomly distributed. Therefore, simple colloidal models are just an approximation.

2.2.2 Second Osmotic Virial Coefficient

A statistical thermodynamic framework can be utilized to account for protein-protein interactions and in turn be used to calculate the second osmotic virial coefficient, B_{22}, which characterizes protein-protein interactions. The protein dispersion osmotic pressure is written as

$$\pi = \frac{RTc_2}{M_2}\left(1 + B_{22}c_2 + \mathrm{L}\right) \tag{2.1}$$

where R is the ideal gas constant, T is the temperature, c_2 is the protein mass concentration, M_2 is the protein molar mass and L encompasses all higher order contributions [25]. The second osmotic virial coefficient accounts for the non-ideal contributions of binary protein-protein interactions. The so-called potential of mean force, $W(r)$, accounts for protein-protein interaction energies. As noted previously there are several contributions that must be considered [26] [27].

$$\mathrm{W(r)} = \mathrm{W_{hard\ sphere}\ (r)} + \mathrm{W_{EDL\ repulsion}\ (r)} + \mathrm{W_{dispersion}\ (r)} + \mathrm{W_{hydration\ water}\ (r)} \tag{2.2}$$

The second osmotic virial coefficient is calculated from the potential of mean force as follows

$$B_{22} = \frac{2\pi N_{\mathrm{Avogadro}}}{M_2}\int \left[1 - e^{-W(r)/k_B T}\right] r^2 dr \tag{2.3}$$

Therefore, the second osmotic virial coefficient directly reflects protein-protein interactions [25] [28] [26]. To assess the second osmotic virial coefficient it is best to consider B_{22} with respect to the predicted hard sphere finite size value, B_{HS}, which is always positive [27].

More formally,

$$\frac{B_{22}}{B_{HS}} - 1 < 0 \qquad \text{overall attractive interactions}$$

$$\frac{B_{22}}{B_{HS}} - 1 > 0 \qquad \text{overall repulsive interactions} \tag{2.4}$$

2.2.3 Characterizing Protein-Protein Interactions

The ideal protein-protein interaction characterization scenario would utilize an experimental technique capable of directly assessing the second osmotic virial coefficient. Fortunately such a method exists – static light scattering. Unfortunately, static light scattering is difficult to implement because sample preparation is difficult, rigorous data analysis is complex owing to the multicomponent nature of protein solutions (especially formulation buffers) and measurements are time consuming therefore abrogating any hope of a high throughput methodology. Sedimentation equilibrium analysis is another potential method, but it is plagued by most of the difficulties that affect static light scattering.

Recently, measurements of the protein collective diffusion coefficient, D, concentration dependence have been considered as an alternative for investigating protein-protein interactions. There is a close relationship between the osmotic susceptibility of a fluid, or the sensitivity to changes in osmotic pressure, and the collective diffusion coefficients associated with the constituent species. However, in addition to this so-called thermodynamic contribution, hydrodynamic interactions also affect the collective diffusion coefficient. All these contributions are captured to first order in the protein concentration by the interaction parameter, k_D,

$$D(c_2) = D_0(1 + k_D c_2 + \ldots). \tag{2.5}$$

Here D_0 is the infinite dilution value of the collective diffusion coefficient sometimes denoted as the self diffusion coefficient and L comprising of all higher order contributions [9] [29]. The particle (protein) hydrodynamic radius can be calculated from the self diffusion coefficient via the Stokes-Einstein relation (see Chapter 4). The classical polymer solution approach for the interaction parameter considers the thermodynamic and hydrodynamic interactions as being separable and ultimately yields the following expression for the interaction parameter [30].

$$k_{\mathrm{D}} = 2B_{22} - k_{\mathrm{s}} - 2\upsilon_{\mathrm{sp}} \tag{2.6}$$

where k_s is the first order correction to the hydrodynamic friction factor and υ_{sp} is the protein partial specific volume in solution. This approach neglects the presence of thermodynamic-hydrodynamic interaction crossterms that are known to exist from more rigorous approaches. Prinsen and Odijk have derived the best estimate of the colloidal dispersion collective diffusion coefficient to date [31]. Their original calculation was carried out using colloidal dispersion volume fraction as the concentration variable. Their prediction for the interaction parameter is as follows

$$k_D \cong \frac{N_{Avogad} V_H}{M_2}\left(1.454 + 4.534\left(\frac{B_{22}}{B_{\mathrm{HS}}} - 1\right)\right) \tag{2.7}$$

where V_H denotes the protein hydrodynamic volume. Both interaction parameter expressions considered here indicate that there is an approximately linear relationship between the interaction parameter and second virial coefficient. Lehermayr and coworkers have demonstrated that that this linear relationship exists for a particular monoclonal antibody formulation [32]. More detailed consideration of the work of Prinsen and Odijk indicates that deviations from this behavior occur when B_{22} is very close in value to the bare hard

sphere value. This occurs when repulsive and attractive interactions are very similar in magnitude.

2.2.4 Specific Ion Effects – Hofmeister Series

As noted previously, protein-protein interactions are influenced by the presence of electrolytes. The *Hofmeister* effect, first noted in 1888, considers specific ion effects that arise in addition to simple ion charge effects. Hofmeister examined the precipitation of egg white proteins with different salts [33]. Lysozyme solubility was found to depend on the chemical nature of the ionic species. Anions and cations are known to follow the so-called direct Hofmeister series (see Figure 2.4), at sufficiently large salt concentrations [34] [35]. At sufficiently low ionic strengths the Hofmeister series is oftentimes observed to be reversed or inverted. These phenomena were recently explained by incorporating ion polarizability and volume effects [36].

Oftentimes ions that appear on the right hand side of the Hofmeister series (red) are commonly denoted as chaotropes or ‘water structure breakers’. These ions are known to compromise protein conformational stability without decreasing colloidal stability [37]. The ions appearing on the left hand side are commonly denoted as kosmotropes or ‘water structure enhancers’. These ions are known to induce protein precipitation at sufficiently high concentrations (‘protein salting out’) while increasing protein conformational stability [37]. For instance, ammonium sulphate precipitation of proteins is a common method for protein separation.

Salt concentration affects electrostatic interaction between molecules. At low concentrations of kosmotropic salt, protein stability is increased by maintaining the electrical double layer. On increasing concentration the electrical double layer thickness decreases with a concomitant decrease in electrostatic repulsion, thus leading to precipitation or ‘salting out’.

Conditions conducive to colloidal instability may render protein solutions cloudy due to protein aggregation and subsequent precipitation. Formulation scientists oftentimes base studies on this series to develop salt mixtures creating conditions optimizing both conformational and colloidal stability.

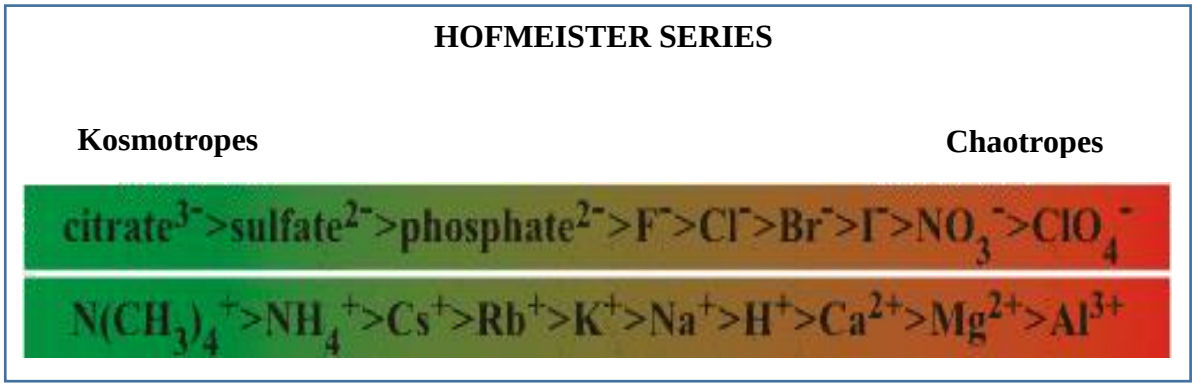

Figure 2.4 An illustration of the Hofmeister series *[34]*.

Chapter 3

Materials & Methods

3.1 Experimental Methods

3.1.1 Stock Solution Preparation

BSA stock solutions of 50mg/ml concentration were prepared in PBS (*Fisher BioReagents*® BP2944-100) at pH 7.4, 50 mM Tris at pH 8.0 and several salt solutions: ammonium sulfate (*Fisher BioReagents*® BP212-212), sodium bromide (*Sigma-Aldrich* 02119-500G) and sodium chloride (*Sigma-Aldrich* S1679-500G). All salt solutions were made in 50 mM Tris pH 8.0.

1.25 grams of BSA was weighed out in a KIMAX 25 mL volumetric flask with the flasks subsequently being filled to the volumetric mark with solvent. Each solution was stored at 2-4°C for a week prior to measurements. Two different BSA sources were considered – *Fisher* and *Sigma-Aldrich*.

3.1.2 Filtration

All buffers and salt solutions were filtered with 0.1 µm alumina-based Anotop™ syringe filters (GE Healthcare Life Sciences). Final BSA stocks were further filtered with 0.02 µm syringe filters of the same composition preceding sample preparation. Potential protein loss following stock solution filtration was monitored by measuring BSA absorbance at 280nm before and after filtration. Any observed protein concentration changes were determined from the Beer-Lambert relation (3.1)

$$A = \varepsilon l c \ . \qquad (3.1)$$

Here A is the absorbance, l is the path length, c is the protein concentration and ε is the protein extinction coefficient.

3.1.3 Characterization of Solutions before Sample Preparation

Prior to sample preparation, stock and filtered solutions were characterized using asymmetric field flow fractionation (FFF) to analyze their aggregation state. A regenerated cellulose membrane, offering minimal protein adsorption, with molecular weight cut-off of 10kDa was used for the FFF separation. FFF is further explained in section 3.2.

3.1.4 DLS

Dynamic light scattering is very sensitive to the presence of aggregates and dust. Large particles can influence protein collective diffusion coefficient determinations; hence meticulous sample preparation is paramount. A *Zetasizer MicroV* (Malvern Laboratories) was used to perform the measurements presented in this thesis. Samples were incubated at 25°C for 15 mins in a heating block prior to measurement for temperature equilibration.

3.1.5 TDA

Taylor dispersion analysis also was used to determine protein collective diffusion coefficients. In this method axial dispersion in laminar tube flow is measured and the protein collective diffusion coefficient is determined via the method first outlined by Taylor [38]. A *Viscosizer 200* (Malvern Laboratories) was used for experiments.

3.2 Protein Dispersion Characterization with FFF

Stock solution aggregation states were characterized by FFF prior to final sample preparation for DLS and TDA analysis. FFF is a hydrodynamic macromolecule/particle separation technique. Particle elution differs from size exclusion chromatography, since smaller particles elute before larger ones. The particle sample is injected into a channel and focused onto a separation membrane with a strong crossflow. During this focusing time, particles begin to segregate by hydrodynamic size in that smaller particles are able to diffuse in the direction against the crossflow. Following a sufficient focusing time, the laminar channel flow is initiated and the fractionated particles are swept out by stream lines of varying velocity with the smallest particles being swept out first owing to their greater diffusion distance from the channel wall with the later eluting particles increasing in hydrodynamic size. The channel dimensions decrease with channel length to further enhance the fractionation capability (see Figure 3.1 [39]).

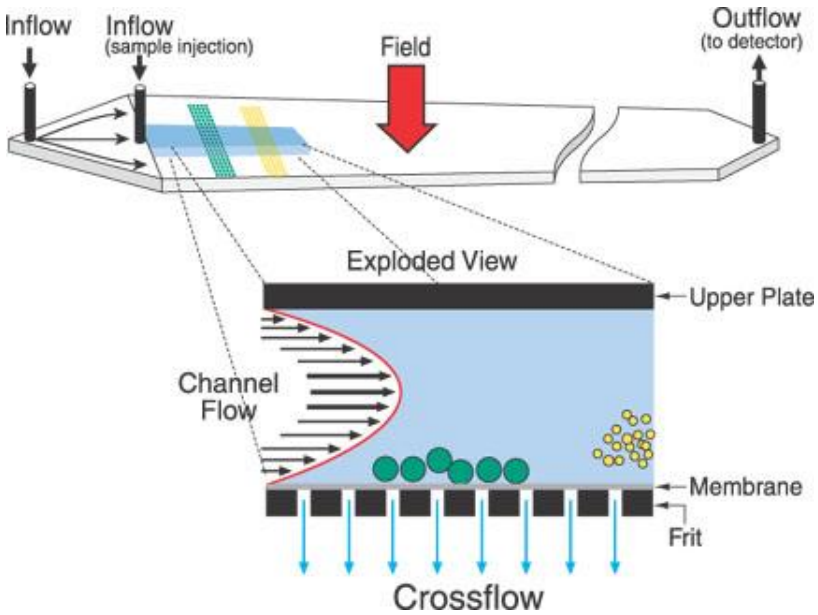

Figure 3.1 A schematic elucidating the principle of FFF *[38]*.

The instrumental configuration consisted of an autosampler (Agilent) and HPLC pump connected to an Eclipse asymmetric field flow fractionation unit (Wyatt Technology). Fractionated samples are characterized with an Optilab refractive index and Dawn Heleos II multiangle light scattering detectors (MALS) from Wyatt Technology. The two detectors provide access to the particle mass concentration and particle size respectively. The instrument is controlled by *Chemstation* software used for setting up different separation methods by varying injection volume, crossflow rate and elution time. Figure 3.2 illustrates a typical FFF instrumental configuration.

Figure 3.2 FFF and ECLIPSE set up along with detectors *[40]* .

3.2.1 FFF Method for Characterizing Protein Dispersions

A standard protein solution separation method was developed using *Chemstation.* The method designed for BSA fractionation starts with an injection flow rate of 0.2ml/min, focusing at 2 ml/min and followed by elution with cross flow rate of 4 ml/min down to 0 over 27 minutes. Table 3.1 lists the steps and duration of each fractionation sequence step. PBS is typically used as the mobile phase for protein dispersion fractionation because it is compatible with both typical samples and the cellulose membrane utilized in the FFF.

Table 3.1 Method in FFF for sample characterization.

Duration (Minutes)	**Mode**	**Start Cross flow rate (ml/min)**	**End Cross flow rate (ml/min)**
2	Elution	0	2
1	Focus	0	0
2	Focus +Injection	0	0
2	Focus	0	0
15	Elution	3	3
5	Elution	3	0

3.2.2 FFF Data Interpretation

FFF chromatograms obtained during this study for different sources of BSA are shown in this section. For these chromatograms, the blue line is the refractive index (RI) detector response and as such is sensitive to the protein mass concentration - a large signal here indicates the presence of significant protein mass. The red and magenta lines are the light scattering (LS) detector responses. These two signals are proportional to the product of the protein mass concentration and the particle molar mass (molecular weight). One should note that the particle may be unaggregated, monomeric protein or protein aggregates. Large concurrent RI and LS detector responses indicate the presence of unaggregated proteins while small RI response coupled with a large concurrent MALS or LS response is a sure indicator of protein aggregates.

Two BSA sources were characterized using field flow fractionation - *Sigma-Aldrich A7030-10G* and *Fisher BSA Fraction V BP1600-100*. The samples were prepared in PBS at a concentration of 50mg/ml as previously described. Figure 3.3 illustrates a typical FFF chromatogram for the *Sigma-Aldrich* BSA. Significant RI and LS peaks (blue and red signals) appear between 11-12 minutes. Analysis of molar mass and hydrodynamic radius from the LS measurements indicate that this peak corresponds to unaggregated, or monomeric, BSA. BSA is known to have hydrodynamic radius of about 3.4nm [41]. The chromatogram was compared to that of a BSA standard provided by Wyatt technology confirming monomeric BSA. The shoulder trailing the primary peak exhibits a low RI signal in conjunction with a significant LS signal consistent with the presence of BSA aggregates – the later elution time supports this interpretation as well, that is, larger particles elute after smaller ones. The LS molar mass measurement confirms this observation.

This sample was assessed over a period of 20 days and an aggregate shoulder was observed each time. Figure 3.4 illustrates separation of the same sample post sonication. It can be seen that sonication had very little, if any, effect on the *Sigma-Aldrich* BSA aggregation state as

presence of aggregates is still seen. Significant quantities of aggregates were still present in the sample after dilution to 10mg/ml and after filtration with 0.02 µm filters (Figure 3.5). Filtration with 0.02 µm filter also had a negligible effect on the aggregation state of *Sigma-Aldrich* BSA in PBS at 50mg/ml as seen in Figure 3.6.

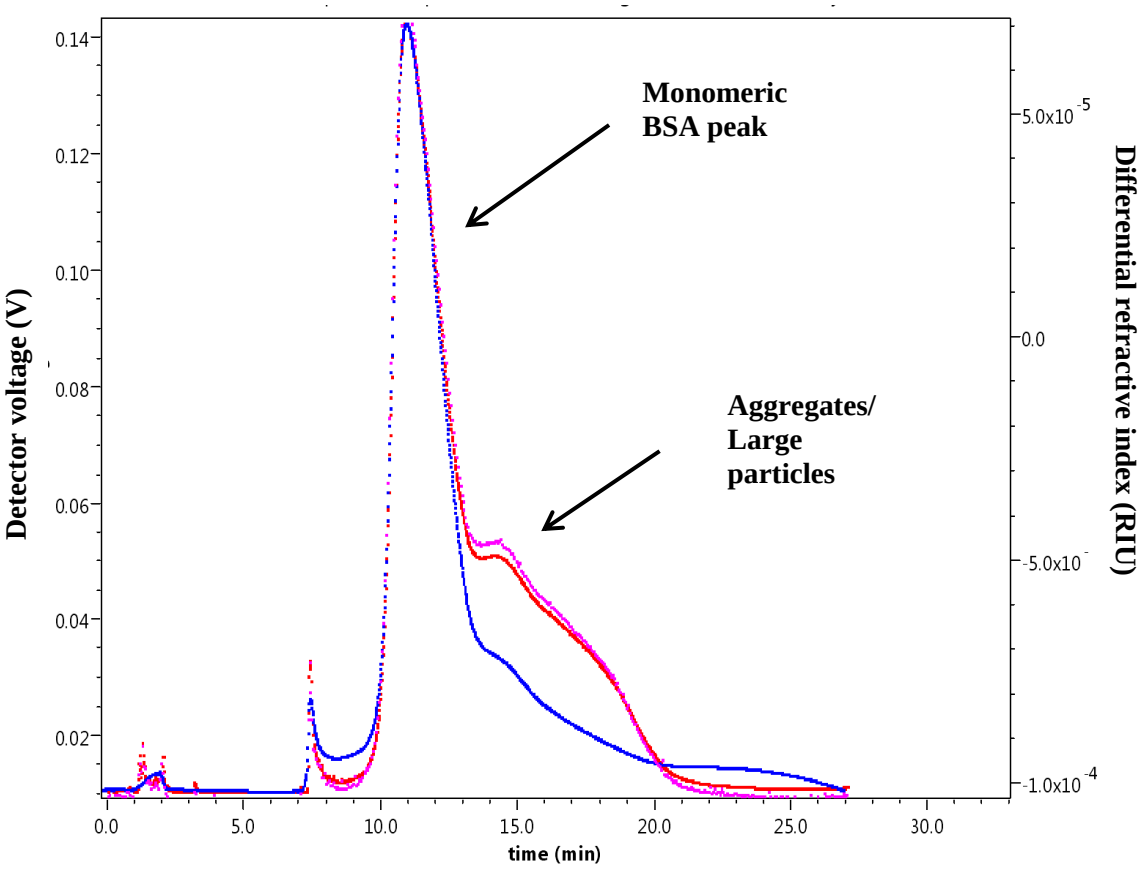

Figure 3.3 FFF separation of *Sigma-Aldrich* BSA in PBS 50mg/ml.

Refractive Index

Dynamic light scattering

Static light scattering

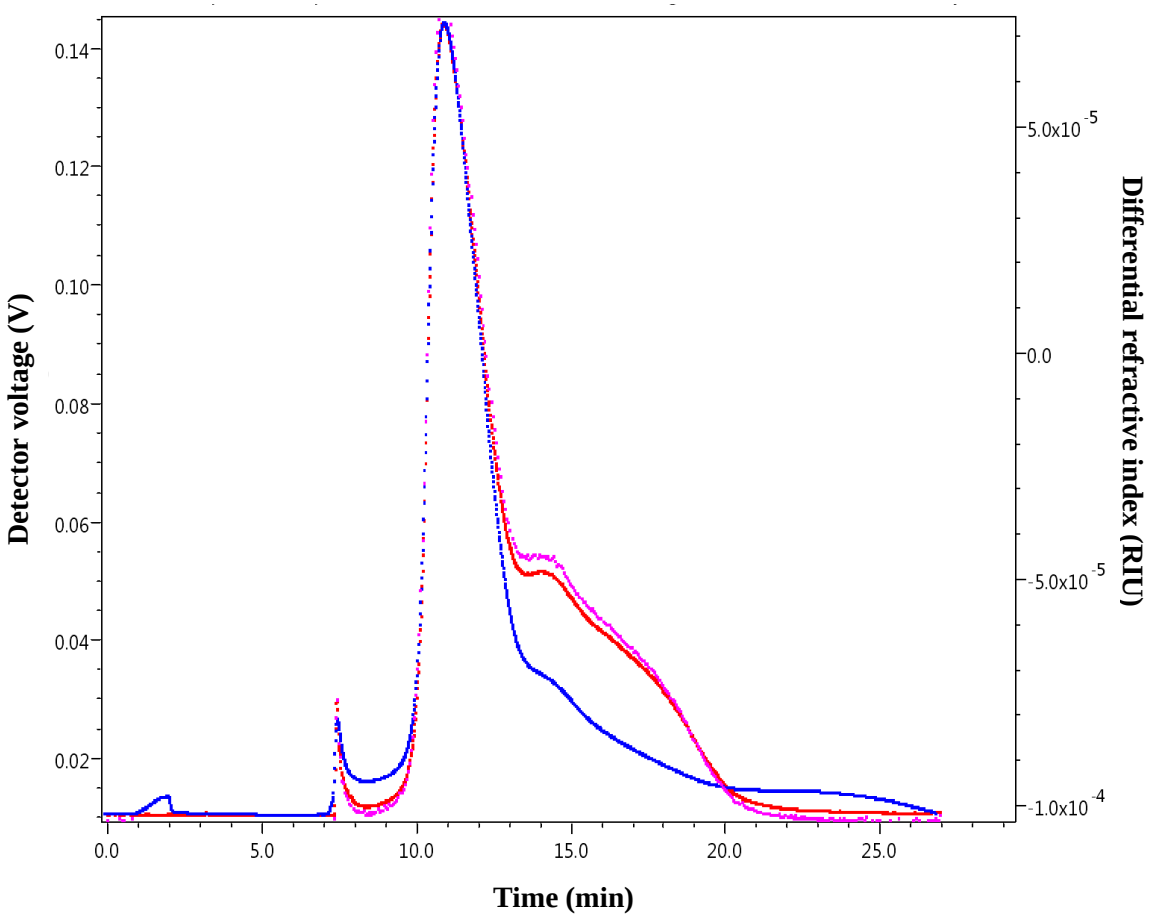

Figure 3.4 FFF separation of *Sigma-Aldrich* BSA 50mg/ml following sonication for 2 minutes. Sonication has very less impact on aggregation state.

Refractive Index

Dynamic light scattering

Static light scattering

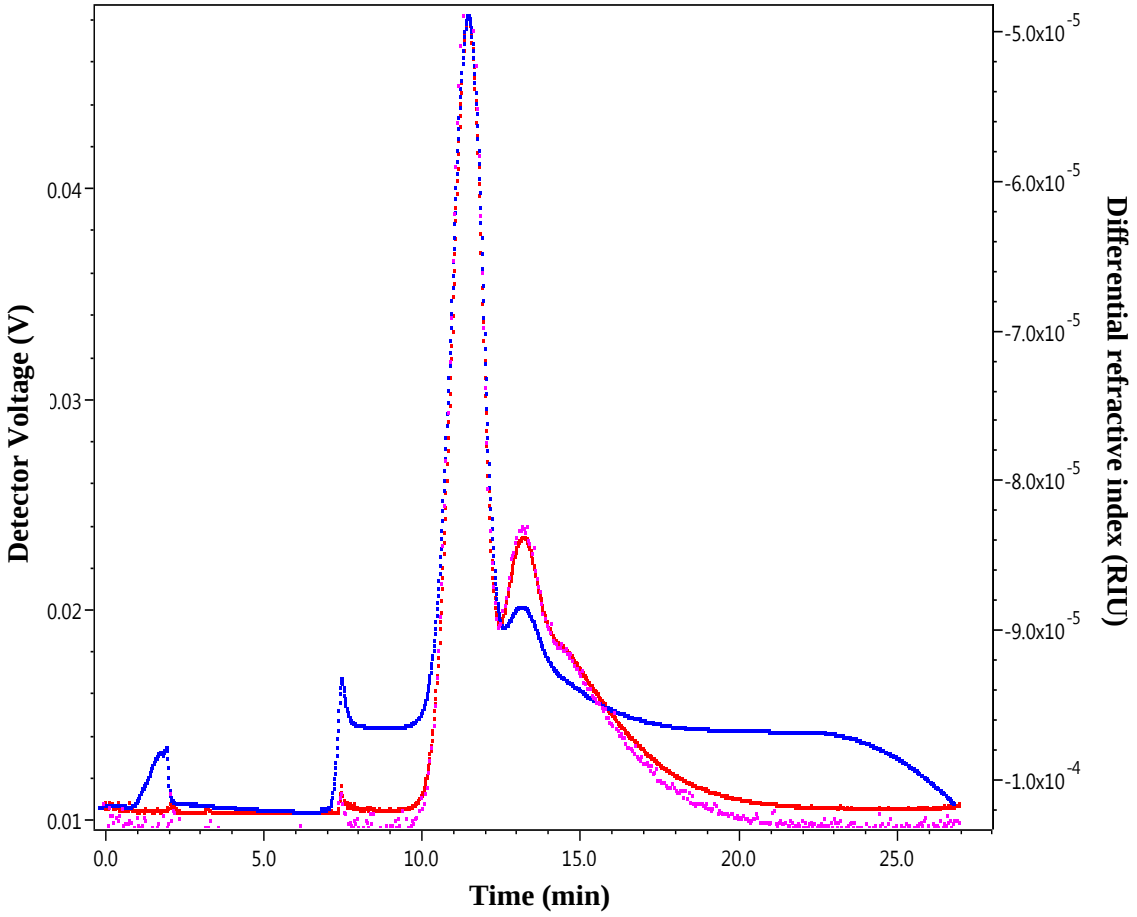

Figure 3.5 FFF separation of *Sigma-Aldrich* BSA 10mg/ml following filtration with a 0.02 µm syringe filter.

Refractive Index
Dynamic light scattering
Static light scattering

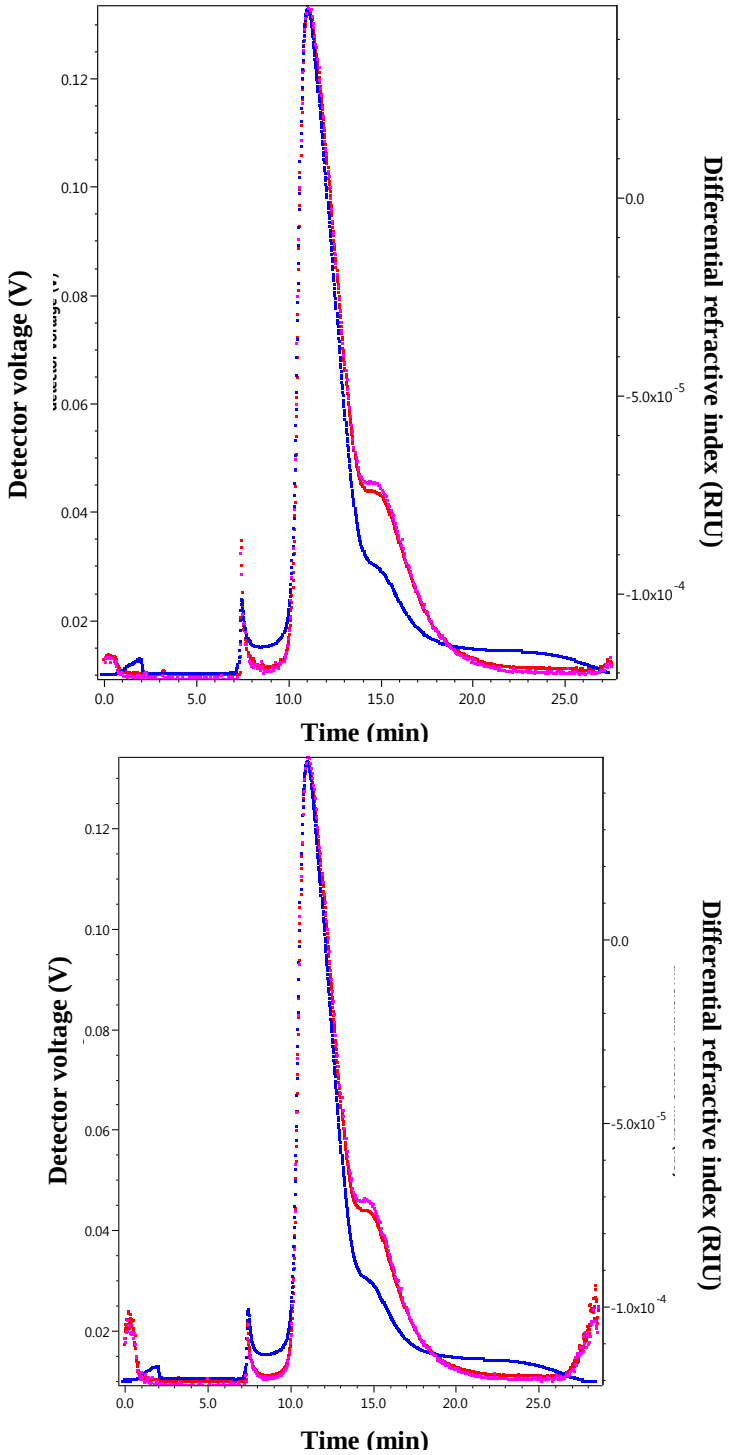

Figure 3.6 FFF of *Sigma-Aldrich* BSA in PBS, 50mg/ml before (above) and post filtration (below).

Refractive Index — Dynamic light scattering — Static light scattering

BSA Fraction *V* from *Fisher* exhibited a much smaller, and almost negligible, shoulder in comparison with the *Sigma-Aldrich* material as shown in Figure 3.7 and 3.8 below. Thus, *Fisher* BSA was chosen for all the experimental measurements reported here as very little aggregation was observed.

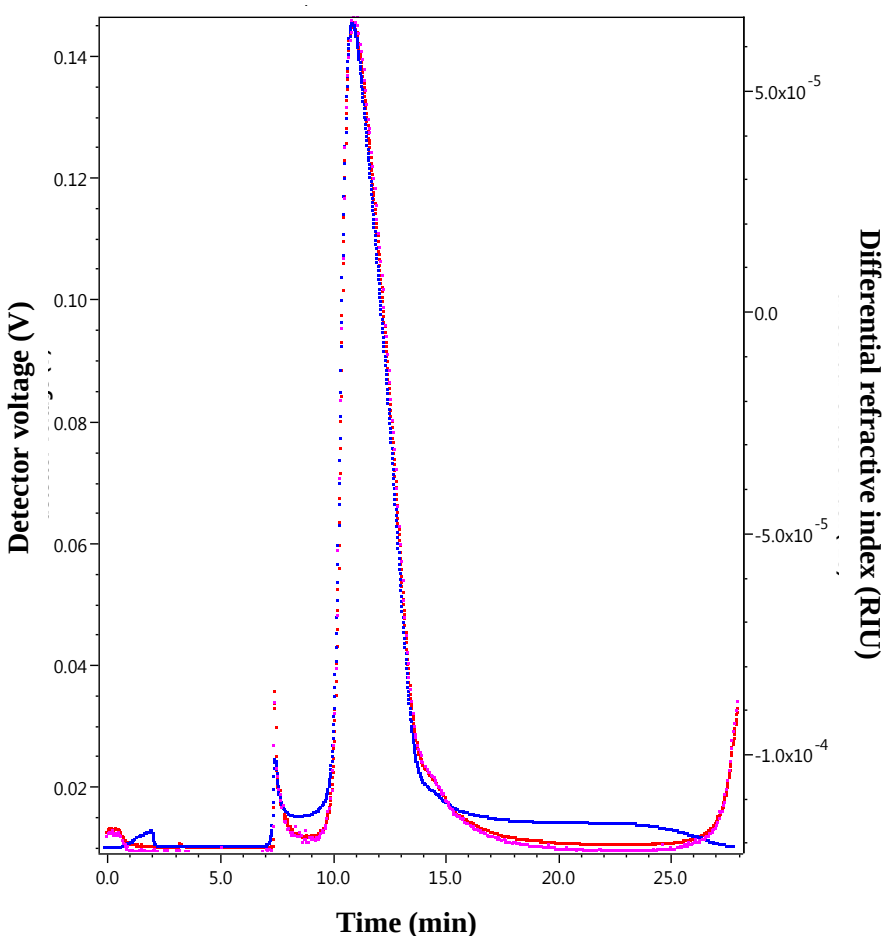

Figure 3.7 FFF separation of *Fisher* BSA in PBS at 50mg/ml stock solution before filtration. Negligible aggregation is seen as compared to BSA from Sigma-Aldrich.

Refractive Index — Dynamic light scattering — Static light scattering

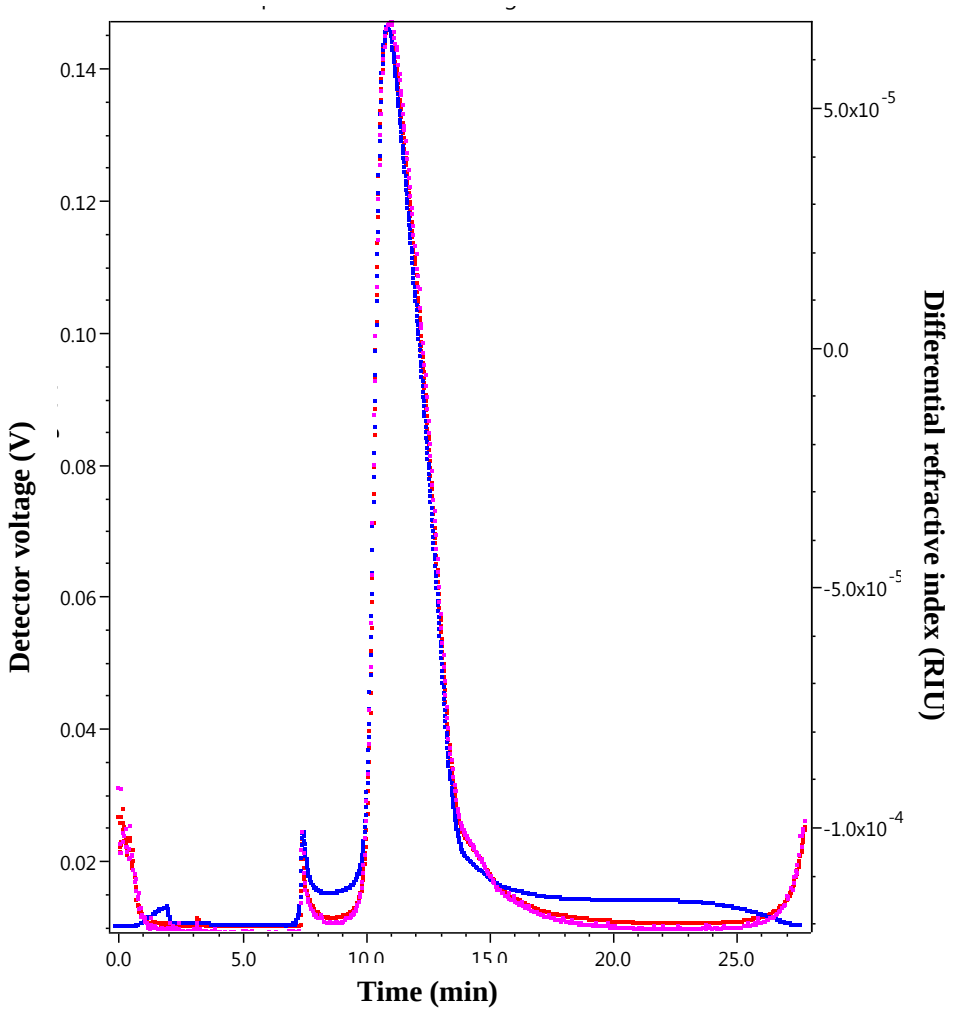

Figure 3.8 FFF separation of *Fisher* BSA in PBS at 50mg/ml post filtration using 0.02 µm filters. Filtration has no significant effect.

Refractive Index — Dynamic light scattering — Static light scattering

Chapter 4

Dynamic Light Scattering

4.1 Introduction

Light scattering from solutions is the result of dielectric constant or refractive index fluctuations that occur due to molecular Brownian motion. The continuous movement causes a Doppler effect, a shift in wavelength of incident light upon scattering, which is related to the particle diffusion coefficient for the case of particle dispersions [42]. For the case of protein solutions, light scattering is a result of fluctuations in the concentration of each component of the solution. Because of their size, protein concentration fluctuations, or local changes in protein concentration, is the principle source of this light scattering and are driven by protein thermal or Brownian motion. DLS methods measure the scattered light intensity fluctuation correlation function. Protein solution DLS measurements will yield the relaxation time of these concentration fluctuations. This relaxation time is directly related to the protein collective diffusion coefficient and, therefore, the protein size via the Stokes-Einstein relation. The relaxation time increases with increasing particle size. Figure 4.1 displays the setup of a DLS instrument. A typical DLS instrument consists of a laser light source, photon detector and digital correlator [43].

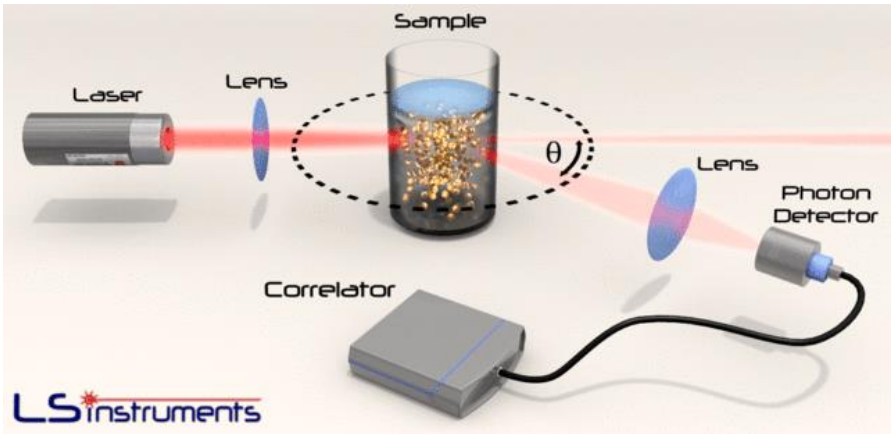

Figure 4.1 Standard dynamic light scattering experimental configuration *[43]*.

4.2 Theory

As stated previously, laser light scattering from protein solutions will exhibit fluctuations in the scattered intensity owing to composition fluctuations primarily resulting from the thermal or Brownian motion of the protein molecules [44] [45]. The scattered light intensity is measured at a fixed angle. The scattered light intensity fluctuation timescale is determined by correlation analysis [9]. The scattered light intensity autocorrelation function is given by

$$g^{(2)}(\tau) = \frac{\langle I(t)\langle I(t+\tau)\rangle\rangle}{\langle I(t)\rangle^2} \tag{4.1}$$

Here $I(t)$ is the intensity of light scattered at time t and τ denotes the delay or lag time. A seemingly 'white noise' intensity temporal trace can be shown to actually contain information regarding the relaxation times associated with refractive index fluctuations driving the observed light scattering. A single relaxation time spectrum, as for the case of monodisperse protein solutions, is shown in Figure 4.2 [43].

At short times the protein dispersion has undergone very little structural rearrangement so the autocorrelation is high, but at sufficiently long times the structural rearrangement has proceeded to the point that the autocorrelation function will begin to decay and at sufficiently long time scales all correlation will be lost.

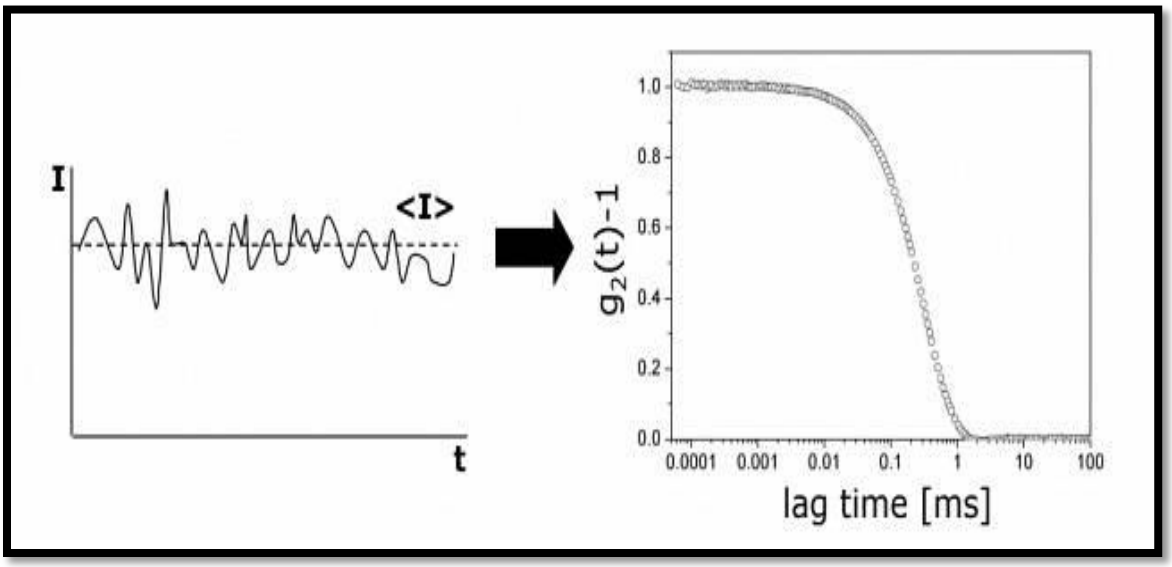

Figure 4.2 Scattered intensity fluctuations and the scattered intensity autocorrelation function *[43]*.

Because small particles diffuse faster than large particles, their scattered light intensity autocorrelation function will decay more rapidly than that for large particles. This is illustrated in Figure 4.3 [42].

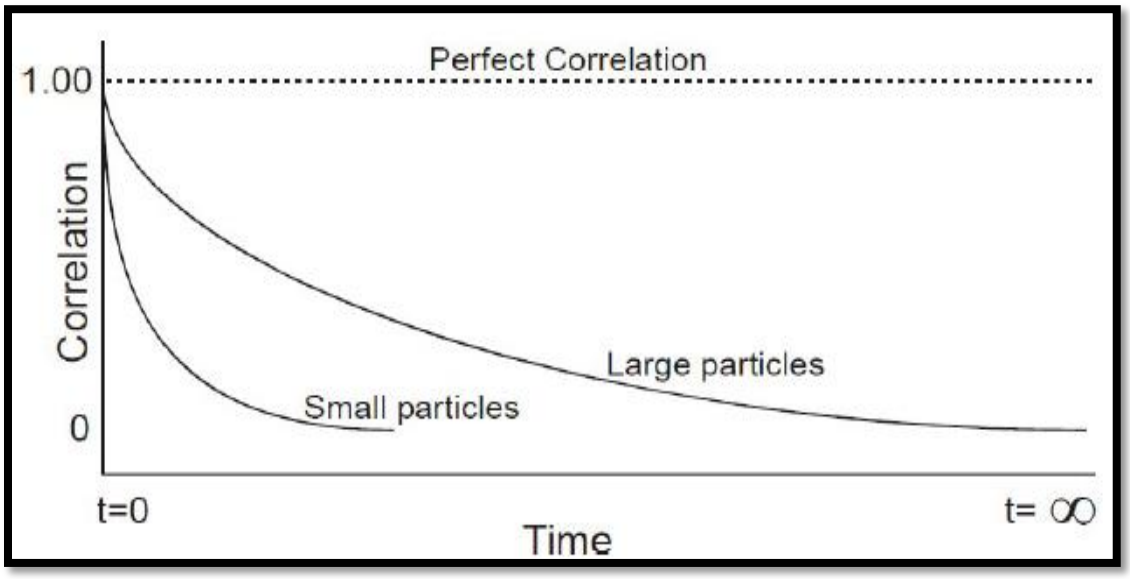

Figure 4.3 Intensity autocorrelation function for small and large particles *[42]*.

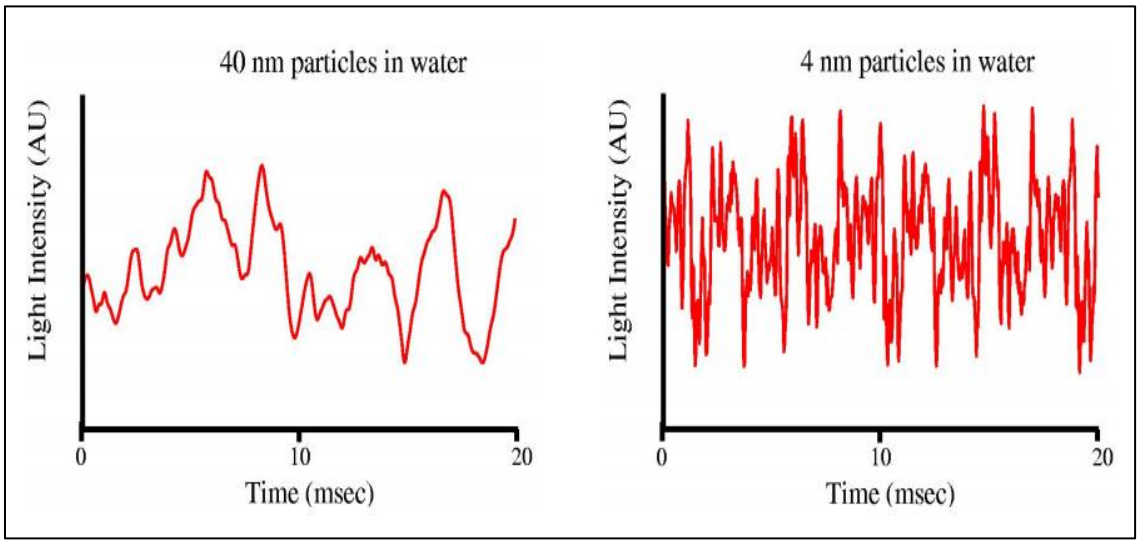

Figure 4.4 Intensity fluctuation timescale for small and large particles *[46]*.

Experimental limitations cause measured scattered intensity autocorrelation functions to differ from the idealized form illustrated in Figure 4.3. These experimental factors include background noise and problems associated with the detection optics limitations. Therefore, the typical experimentally determined scattered intensity autocorrelation function will exhibit the following form:

$$g^{(2)}(\tau) = B + \beta e^{-2q^2 D\tau} \tag{4.2}$$

where B is the baseline, β is the correlation amplitude at zero delay, q is the scattering vector and D is the particle (protein) collective diffusion coefficient [47] [48] [49] . The scattering vector is defined as follows:

$$q = \frac{4\pi n}{\lambda_0} \sin(\theta/2). \tag{4.3}$$

Here n denotes the solvent refractive index, λ_0 is laser wavelength *in vacuo* and θ is the scattering angle. The infinite dilution particle (protein) diffusion coefficient, D_0, is related to the particle (protein) size via the Stokes-Einstein relation:

$$D_0 = \frac{k_B T}{6\pi\eta R_H} \tag{4.4}$$

Here k_B is Boltzmann's constant, T is temperature, η is the solution viscosity and R_H is the particle (protein) hydrodynamic radius. The term hydrodynamic radius denotes the fact that the radius is measured by a hydrodynamic method; the proteins are dispersed in aqueous media whose presence influences the measurement. One should note that application of the Stokes-Einstein relation requires the assumption of spherical shape [50].

4.3 DLS Data Analysis

The simplest method for analyzing the scattered light intensity autocorrelation function would be to apply equation 4.2 to the collected data. However, this approach will fail for essentially every data set collected owing to experimental and sample limitations. Equation 4.2 would only be valid if the sample was absolutely monodisperse and there were no experimental artifacts owing to optical train, detector and electronic random errors. Small deviations will lead to the presence of a stretched exponential. A moment analysis of equation 4.2 provides access to mean relaxation time and the variance (width) of the relaxation time distribution. It is also known as the Cumulant method [51]. The presence of aggregates, even a small amount, will lead to an increase in the mean relaxation time thereby obscuring the relaxation time of the monomeric proteins which is the focus of this study. An alternative approach is to utilize regularization methods to 'invert' the correlation function into a relaxation time distribution which can be converted to size distribution. Regularization methods utilize the so-called principle of parsimony to ensure that the relaxation time spectrum is not overinterpreted to yield an unnecessarily complex relaxation time distribution [52]. These methods are well established and robust. The results presented in this thesis will utilize the monomeric protein relaxation time as determined by regularization analysis to remove the contribution from the small population of protein aggregates present in all of the samples considered here.

4.4 Dynamic Light Scattering Characterization of Particle and Protein Dispersions

This section describes and compares dynamic light scattering collected for polystyrene latex and protein dispersions based on both cumulant method and regularization to shed light on the differences. The former system is ideal in that it is a monodisperse dispersion of spherical particles an order or magnitude larger than typical proteins. This significantly larger size will

provide much stronger light scattering signal than that found for proteins since the scattered intensity is proportional to the square of the particle volume [42].

4.4.1 Polystyrene Latex Spheres

Figure 4.5 shows a typical scattered intensity autocorrelation function measured for our model polystyrene latex spheres at a volume fraction of ~ 0.0625%. Polystyrene lattice hydrodynamic size was determined to validate the method and system prior to BSA measurements. A typical regularization inversion of the collected data yields the intensity weighted particle size distribution (radius in nm) illustrated in Figure 4.6. The regularization routine estimates the polystyrene latex particle diameter as 22.8 ± 0.3 nm, while cumulants analysis yields a value of 21.9 nm. Both methods indicate the polystyrene latex dispersion is very monodisperse. The manufacturer, ThermoScientifc, reports a certified value of 21 ± 2 nm in excellent agreement with the values measured with the BTEC Zetasizer µV.

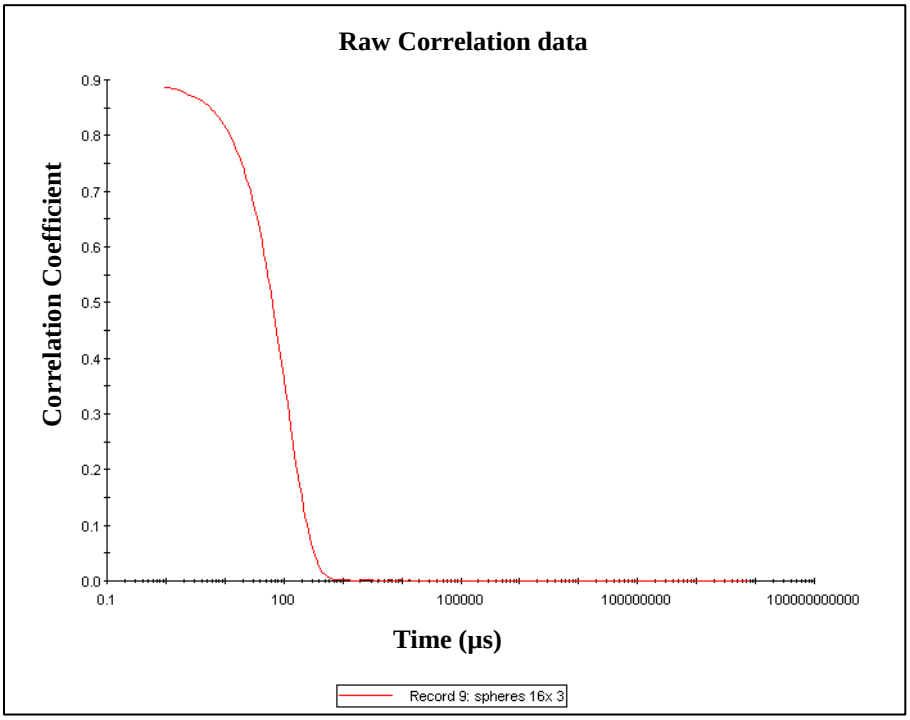

Figure 4.5 Scattered light autocorrelation function measured for 20 nm in diameter polystyrene latex spheres.

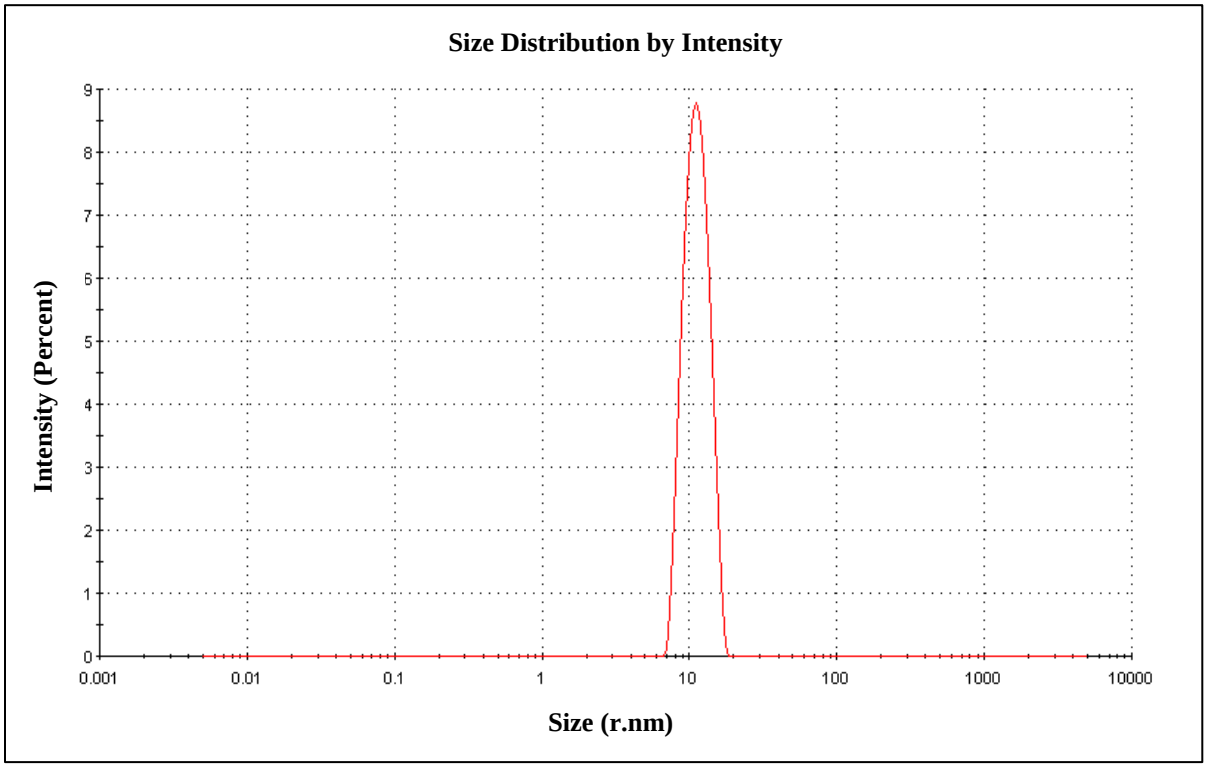

.

Figure 4.6 20 nm polystyrene latex intensity weighted size distribution as measured by dynamic light scattering. The y axis shows intensity and the x axis shows the radius in nanometers.

4.4.2 BSA in PBS and 50 mM Tris/2 M Ammonium Sulphate

Although the current study has considered BSA dispersed in numerous solvents, in this section the focus will be on the dynamic light scattering data collected for two different solvents, PBS and 50 mM Tris/2 M ammonium sulphate, where the former yields repulsive protein-protein interactions compared to the latter inducing the attractive forces. A typical scattered light intensity autocorrelation function measured for BSA dispersed in PBS is shown in Figure 4.7. The correlation function is well behaved in that it exhibits a single relaxation time or decay rate.

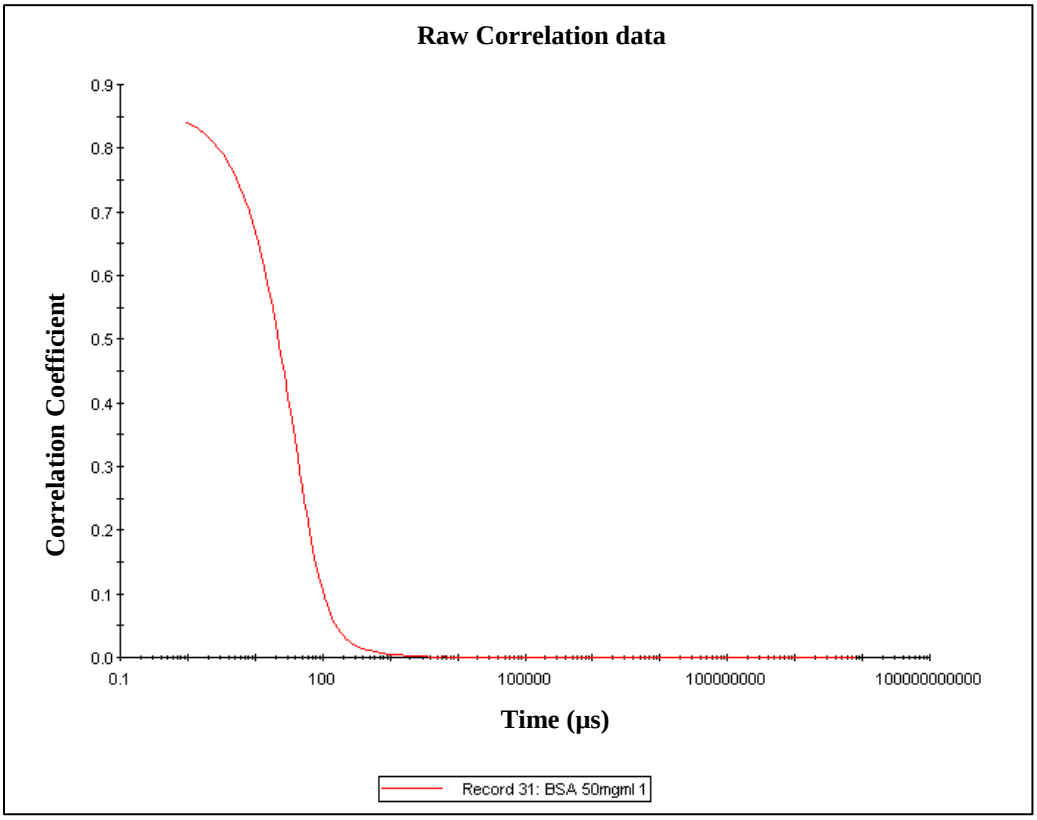

Figure 4.7 Scattered light intensity autocorrelation function for BSA in PBS, 50mg/ml.

The regularization analysis yields the following intensity weighted size distribution (Figure 4.8) illustrating that a population of aggregates is present. As mentioned earlier, the light scattering intensity is proportional particle volume so the aggregate peak shown here is indicative of a relatively small number of aggregates. Cumulants analysis will reflect the presence of the aggregates by reporting a mean radius that is larger than that measured by the regularization method as mentioned in the Data Analysis section of this chapter therefore the monomeric peak size as determined by the regularization method is reported throughout this document.

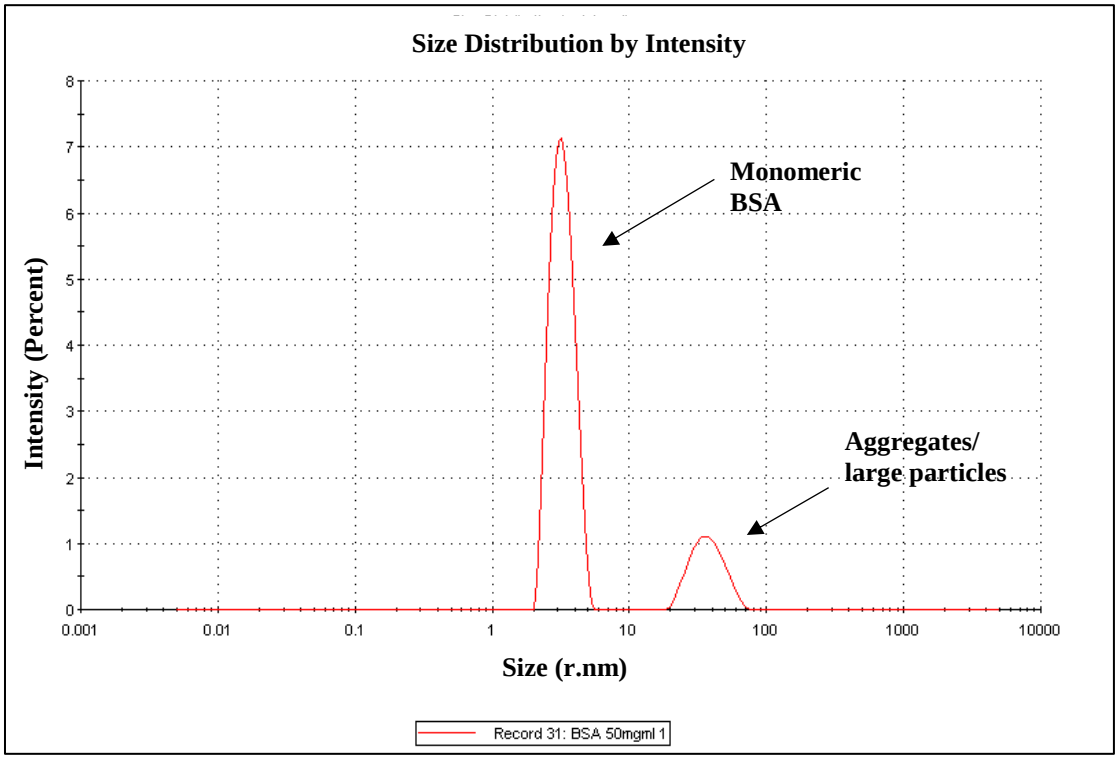

Figure 4.8 Size Distribution by Intensity for BSA in PBS 50mg/ml. The monomeric peak for BSA is at around 3.8nms. Smaller peak close to 100nm represents aggregates or large particles such as dust.

A scattered light intensity autocorrelation function measured for BSA dispersed in 50 mM Tris/2 M ammounium sulphate is shown in Figure 4.9. This correlation function indicates that there are two well separated relaxation times indicative of the presence of two species, monomeric BSA and larger aggregates when attractive protein-protein interactions are operative. Sample preparation was difficult in that our standard 50 mg/ml stock solution approach failed with significant precipitate being present. Further dilution to 25 mg/ml dissolved the precipitate but yielded a fairly turbid solution. Subsequent dilution to 10 mg/ml provided a visibly clear solution, but there was a high likelihood that some irreversibly aggregated material may still exist as confirmed by the DLS measurements shown here.

The 50 mM Tris/2 M ammonium sulphate BSA collective diffusion coefficient data presented later in this chapter were collected for a stock solution originally formulated at only 10 mg/ml BSA concentration to minimize the formation of BSA aggregates.

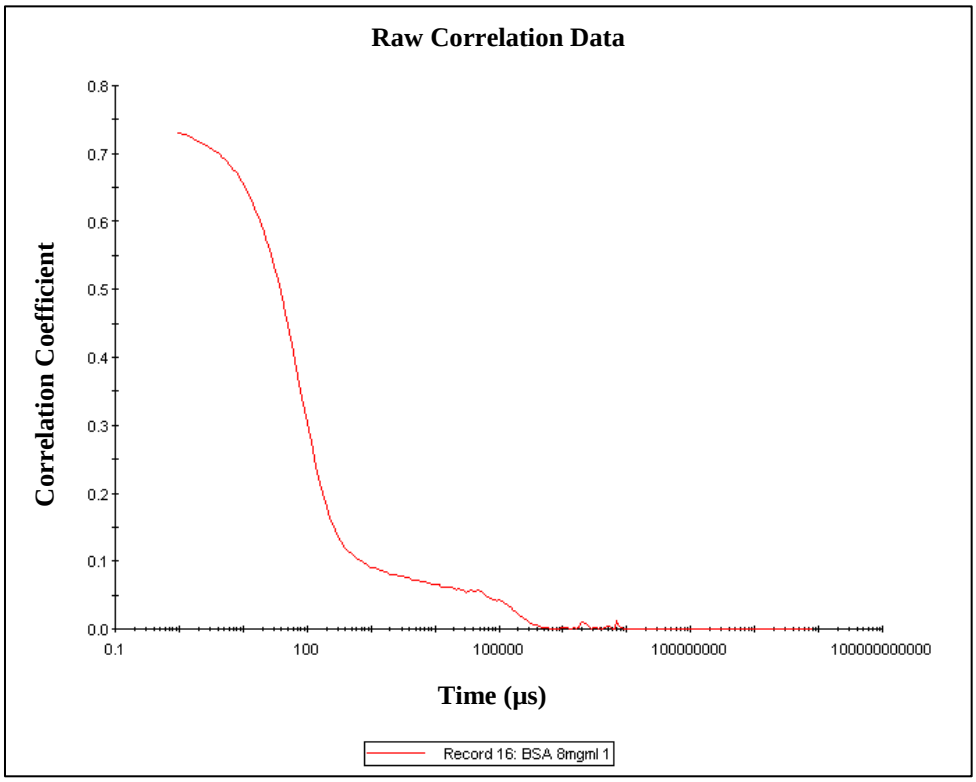

Figure 4.9 Correlation function for 8mg/ml of BSA in 50mM Tris/2 M ammonium sulphate.

The regularization analysis yields the following intensity weighted size distribution (Figure 4.10) illustrating that two populations of aggregates are present – one that is similar in size as that found for BSA in PBS as well as some material consisting of larger aggregates.

Since the light scattering intensity is proportional to particle volume so the aggregate peaks shown here are indicative of a relatively small number of aggregates – especially the large aggregate case. The increased monomeric BSA size is indicative of attractive protein-protein interactions in 2 M ammonium sulphate. This shows impact of solvent type on interactions.

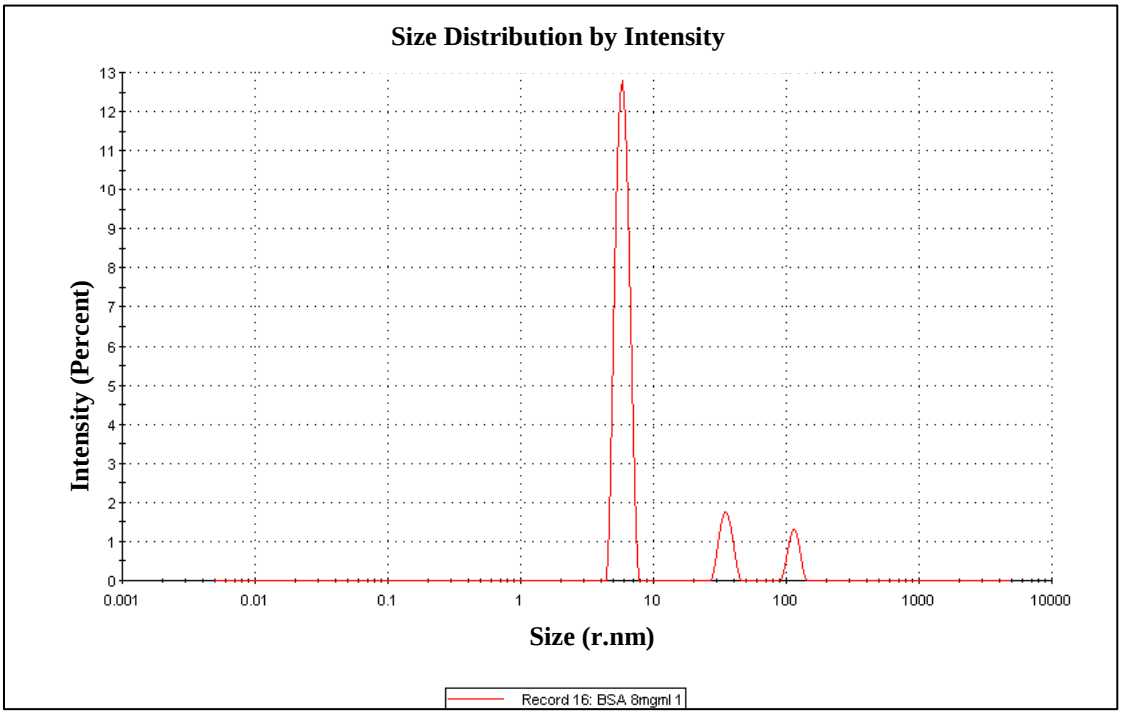

Figure 4.10 Size Distribution by Intensity for BSA 8mg/ml in 50mM Tris /2 M ammonium sulphate.

4.5 Protein Solution Collective Diffusion Coefficient Measurements

While the previous section compared DLS data for polystyrene latex and protein dispersions, here the effect of buffer composition on the protein collective diffusion coefficient concentration dependence is considered for several representative solution compositions.

Diffusion coefficients for BSA were calculated from the monomeric peak size obtained from regularization (See Appendix A for values of diffusion coefficients). BSA is known to have a diffusion coefficient of 6.3 x 10e-7 cm^2/s when dispersed in NaCl solution of ionic strength 0.1 M measured by DLS [41].

4.5.1 Comparison of Different Buffer Compositions

The solution compositions considered here include 50 mM Tris (pH 8.0), PBS (pH 7.4) as well as 1 and 2 M ammonium sulphate solutions prepared in 50 mM Tris (pH 8). All the solutions considered here will yield negatively charged BSA since its pI of 4.7 is lower than the buffer pH. Collective diffusion coefficient versus concentration is presented for each buffer composition in figure 4.11.

The BSA collective diffusion coefficient increases with increasing BSA concentration for both Tris and PBS with Tris exhibiting a stronger positive slope than PBS. Under these conditions, due to electrostatic repulsions, proteins will diffuse faster owing to the repulsive interactions. The observed infinite dilution diffusion coefficient, or self diffusion coefficient (Chapter 2) variation results from changes in solvent viscosities. For example, the approximately 20% change in the infinite dilution diffusion coefficient (Figure 4.11 y –axis) observed when comparing BSA in Tris and Tris/1 M ammonium sulphate solutions correlated with a 20% change in buffer viscosity. The absolute viscosities for Tris and 1M ammonium sulphate taken into account here are 1.01 and 1.21 cP respectively [53]. Thus, the more viscous Tris/1 M ammonium sulphate exhibits a smaller infinite dilute diffusion coefficient value for BSA as it tends to diffuse slower.

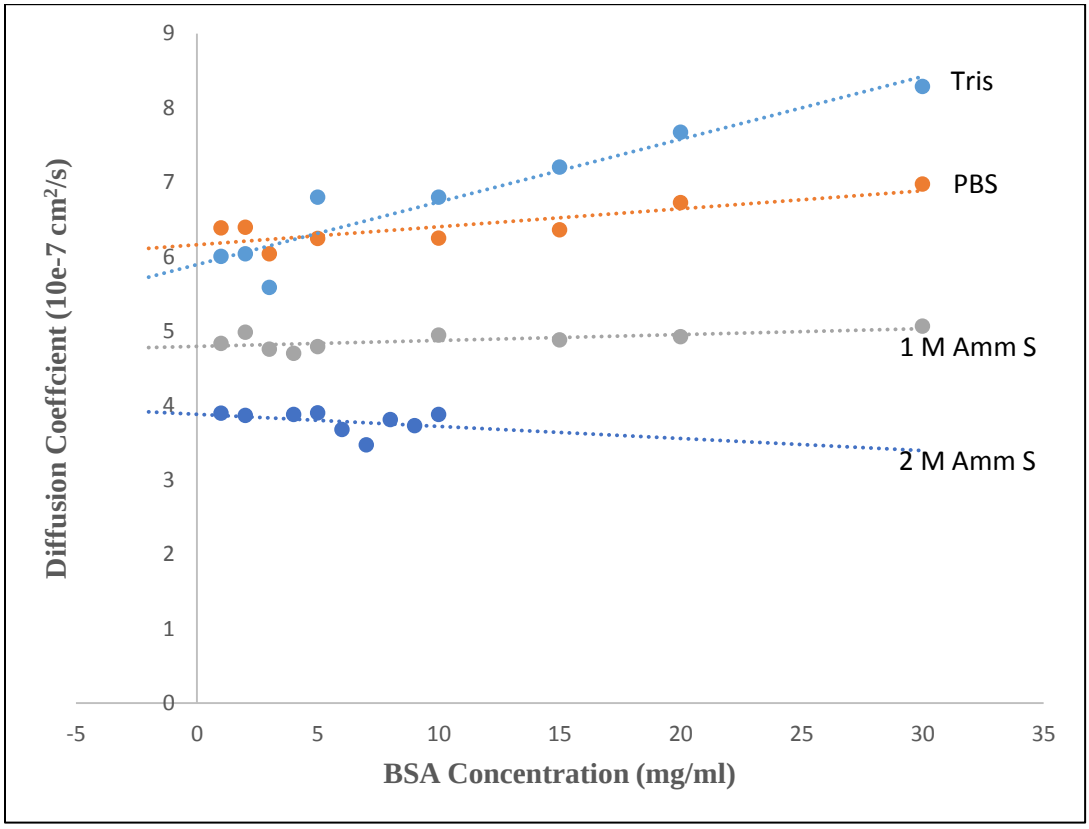

Figure 4.11 Concentration dependence of diffusion coefficient for different solvents.

.

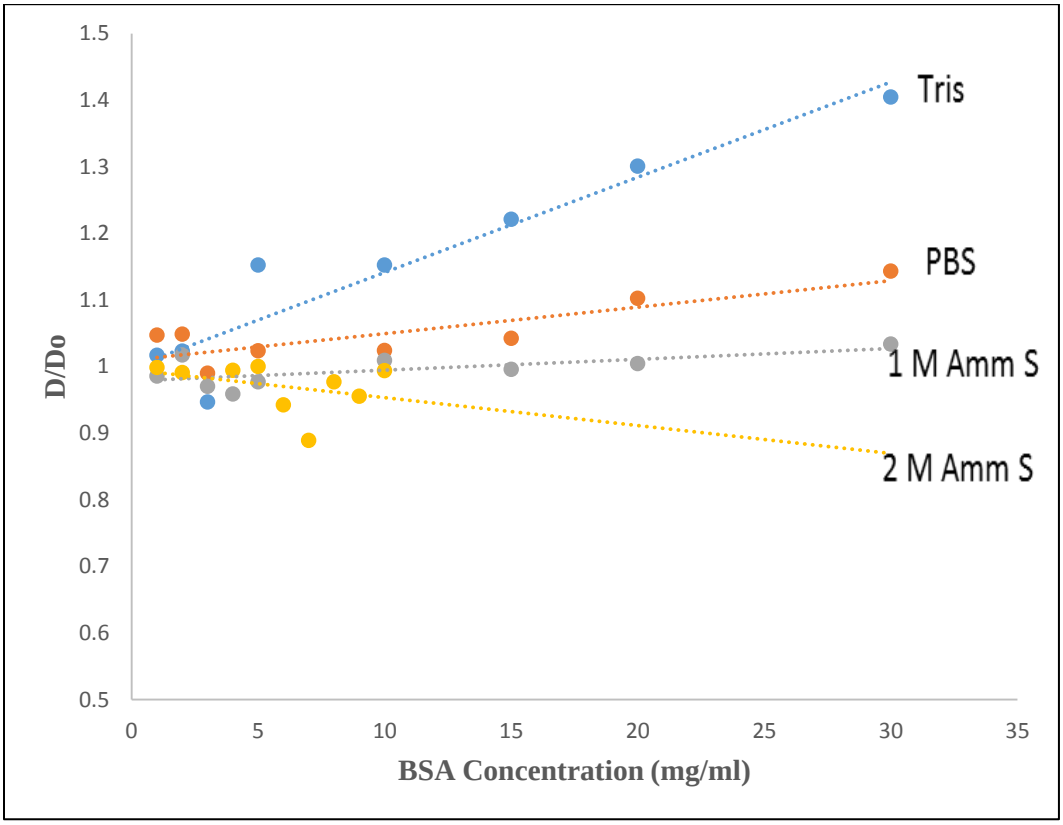

Figure 4.12 Dynamic Debye Plot to determine interaction parameter k_D from the slope.

In order to highlight protein-protein interaction differences a dynamic Debye plot (Figure 4.12) is created wherein the normalized collective diffusion coefficient is plotted as a function of concentration in order to eliminate the role of solution viscosity. Recalling equation (2.5) which is shown for clarity below

$$D = D_O\,[1 + k_D C + \cdots] \tag{4.5}$$

It is apparent the varying slopes indicate different values of the protein-protein interaction parameter k_D. The measured k_D values obtained for different solvents are shown in Figure 4.13.

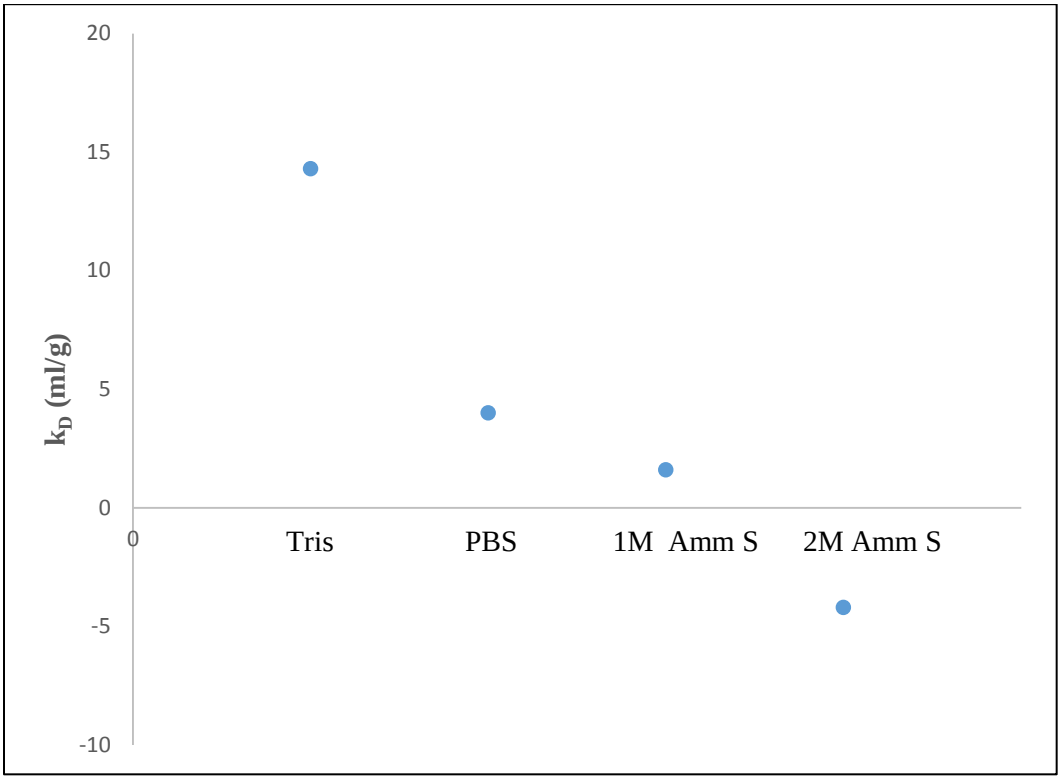

Figure 4.13 Interaction parameter k_D for different solvents. Y- axis represents the values for k_D. X-axis shows different solvents for the respective data points for k_D.

The lower k_D for BSA in PBS than observed for Tris likely arises from the presence of 127 mM NaCl in PBS. NaCl will decrease electrostatic repulsion via a decrease in the electrical double layer thickness. For BSA in 50mM Tris/1M ammonium sulphate k_D approaches a negative value indicative of a decrease in electrostatic repulsion owing to the presence of the ammonium sulfate at high concentrations thereby greatly decreasing the electrical double layer thickness in comparison with that found for the case of 50 mM Tris alone. A negative k_D was observed for 50 mM Tris/2M ammonium sulphate thereby indicating attractive interactions which is in agreement with difficulties observed with high concentration solution preparation in the buffer.

4.5.2 BSA in Ammonium Sulphate

Ammonium sulphate concentration (0.1, 0.2, 0.5, 1 and 2 M) was varied in 50 mM Tris. Ammomiun sulphate was considered to highlight the impact of a highly kosmotropic salt on protein-protein interactions. Initial BSA stock concentration for each solution was 50mg/ml. The 2 M ammonium sulphate stock solutions was very cloudy as stated earlier compared to lower ionic strength solutions. This solution was allowed to dissolve for an additional day and stored at 2-4°C. BSA precipitation was observed for this case.

When a sufficiently concentrated protein solution is kept at conditions below its 'cloud-point' temperature the solution splits into two immiscible forms leading to phase separation and sedimentation of the coacervates [54]. 2 M ammonium sulphate solution was further diluted to 25mg/ml where it was observed to remain turbid with slight precipitation. To avoid large aggregates which could cause artifacts in the DLS measurements the solution was further diluted to 10mg/ml.

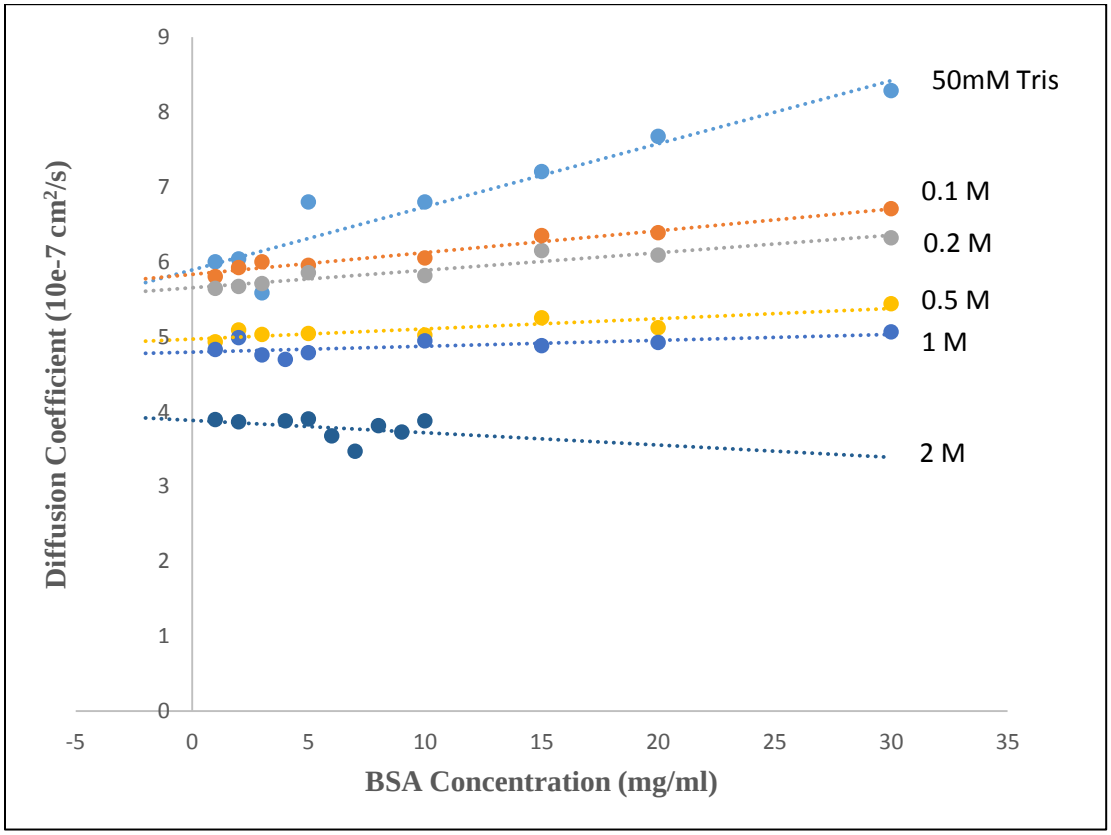

Figure 4.14 Collective diffusion coefficient. 50mM Tris compared to different concentrations of ammonium sulphate.

The effect of ammonium sulphate concentration on the protein collective diffusion is shown in Figure 4.14. Once again the change in the infinite dilution coefficient value is well correlated with changes in solvent viscosity. The protein collective diffusion coefficient concentration dependence begins to weaken as ammonium sulphate is added to the solution resulting from a decrease of the electrical double layer repulsion owing to concomitant diminishment of the electrical double layer thickness. Eventually electrostatic repulsion is entirely screened and attractive interactions become prominent. This is most likely the scenario for the case of the 1 M solution and definitely the situation for the 2 M solution as

indicated by the negative protein collective diffusion coefficient concentration dependence. The electrostatic screening increases the hydrophobic nature of the BSA surface thereby leading to attractive protein-protein interactions driven by the so-called hydrophobic effect. Such conditions act as precursors for protein aggregation. The determined k_D values are shown in Figure 4.15.

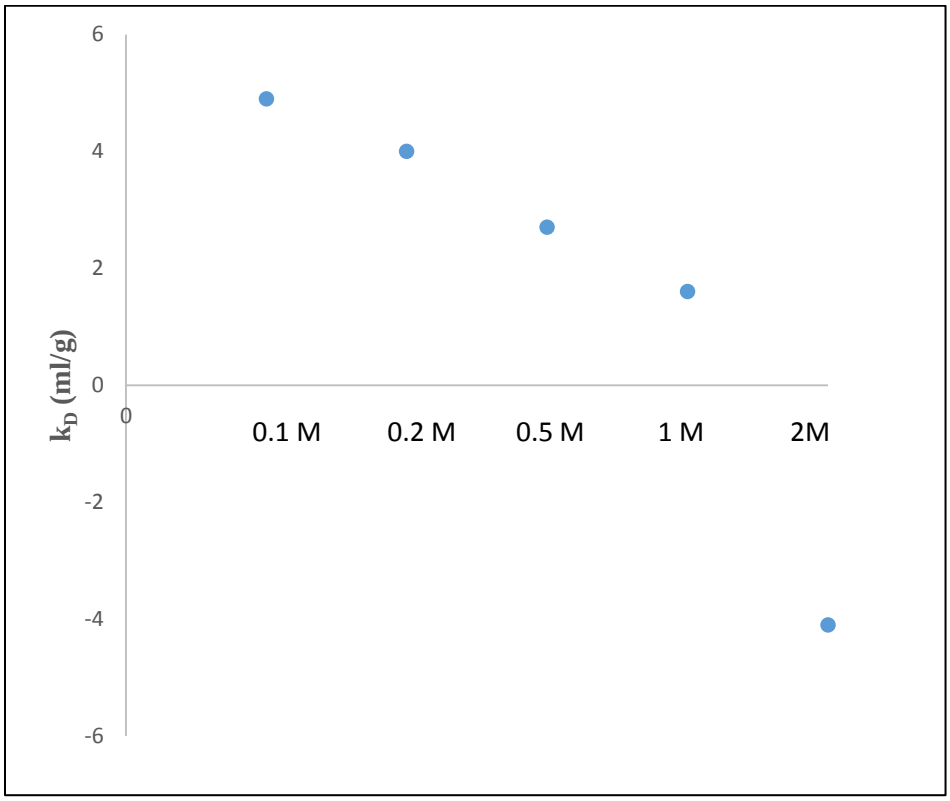

Figure 4.15 Interaction parameter k_D for BSA dispersed in different concentrations of ammonium sulphate. X-axis represents different concentrations of ammonium sulphate for the respective k_D data points.

4.5.3 Comparison of Different Salts

Hofmeister effect (Chapter 2) was assessed by comparing ammonium sulphate, NaCl and NaBr at the same molarity of 1M – keep in mind that the ammonium sulphate is at a different ionic strength for this case and as such it is a much more effective screener of electrostatic repulsion. All the solutions were at pH 8.0 giving BSA a negative charge. Figure 4.16 shows the protein collective diffusion coefficient concentration dependence for all three solutions, and the respective k_D values are plotted in Figure 4.17. As expected ammonium sulphate has a greater effect on the observed behavior based on its position in the Hofmeister series and the fact that it is present at greater ionic strength. NaCl and NaBr are in their expected positions as well with NaCl being a more effective screener of electrostatic repulsion. This phenomenon is driven by the fact that Br^- is a more polarizable anion than Cl^- and as such will be a higher affinity coion for the Na^+ counterions that are attracted to the negatively charged BSA surface.

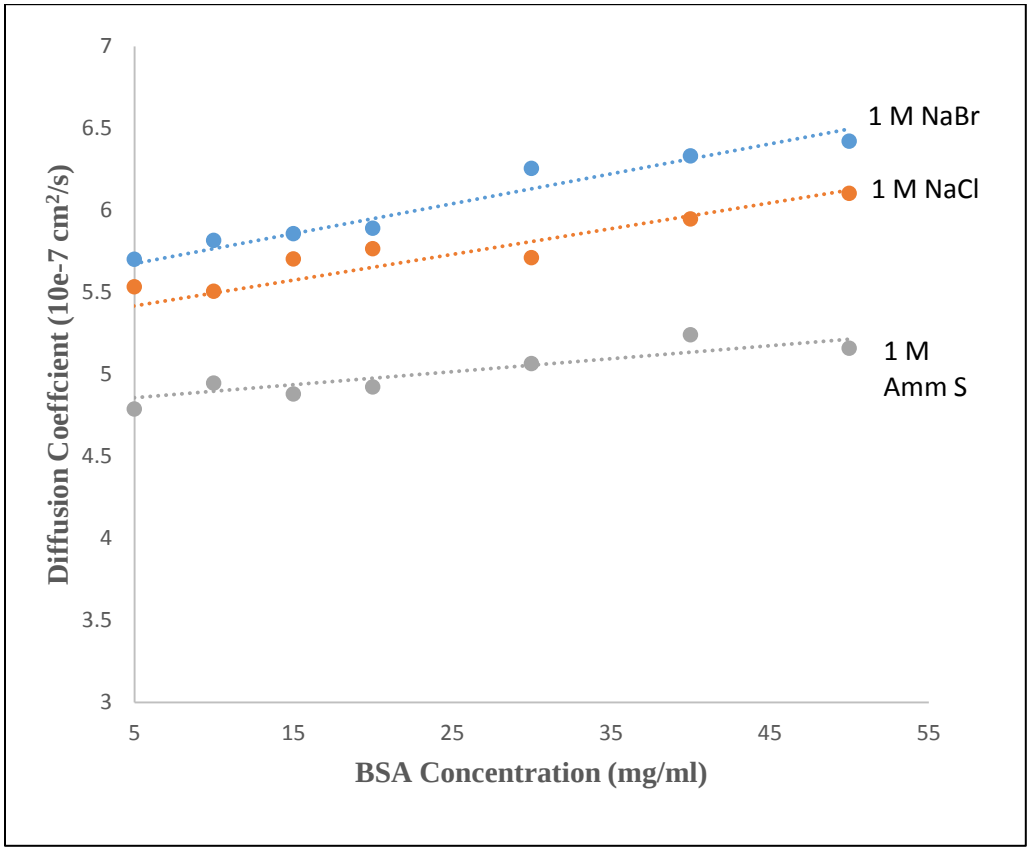

Figure 4.16 Comparison of diffusion coefficient of NaBr, NaCl and ammonium sulphate.

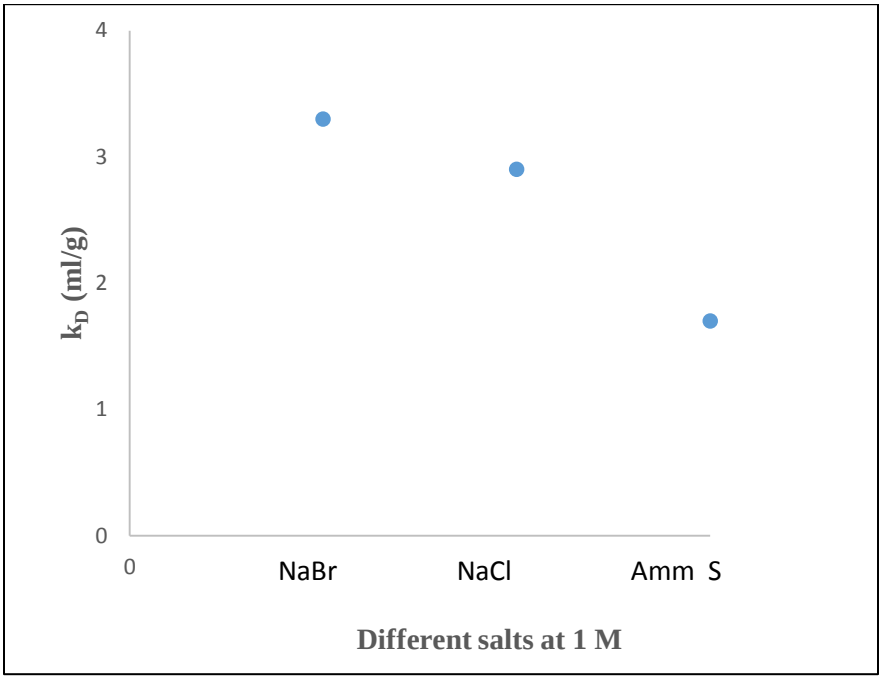

Figure 4.17 Comparison of k_D values for NaBr, NaCl and ammonium sulphate.

This chapter demonstrated the utility of using dynamic light scattering to characterize protein-protein interactions. The BSA collective diffusion coefficient concentration dependence was determined for BSA dispersed in 50 mM Tris solutions both in the absence and presence of salts such as ammonium sulphate, sodium chloride and sodium bromide in order to investigate the impact of so-called specific ion effects on protein-protein interactions. The two prime phenomena noted here were (a) the effect of ion concentration and (b) the effect of ion type. Ammonium sulphate solutions of varying concentration were used to demonstrate the effect of ion concentration on electrostatic repulsion and thereby protein-protein interactions. Electrostatic repulsion is observed to decrease with increasing ammonium sulphate concentration as expected. The role played by ion type was shown by considering NaCl and NaBr in conjunction wherein protein-protein interactions were found to be in agreement with the predictions of the Hofmeister series.

Chapter 5

Taylor Dispersion Analysis

5.1 Introduction

British fluid dynamicist G. I. Taylor was the first researcher to describe the dispersion of a dissolved solute following its introduction to a laminar circular pipe flow in 1953 [38]. Taylor established a relationship between the observed solute dispersion and the solute collective diffusion coefficient for the case wherein axial convection dominates axial diffusion. Taylor first demonstrated the method of so-called Taylor Dispersion Analysis (TDA) by determining the potassium permanganate collective diffusion coefficient in aqueous solutions. Aris further extended Taylor's theoretical work in 1955 [55]. Recent investigations have demonstrated TDA is a robust method for fast and accurate diffusion coefficient measurements. More recently, TDA has been compared to traditional DLS as a hydrodynamic sizing technique [56].

5.2 Theoretical Overview

G.I. Taylor considered the solution of the following convective diffusion equation for laminar flow in a circular tube [57]

$$\frac{\partial c}{\partial t} + u(r)\frac{\partial c}{\partial z} = D\left(\frac{\partial^2 c}{\partial z^2} + \frac{1}{r}\frac{\partial}{\partial r}\left(r\frac{\partial c}{\partial r}\right)\right) \tag{5.1}$$

where c is the solute concentration, $u(r)$ is the velocity profile, D is the solute diffusion coefficient, r is the radial position, z is the distance along the tube and t is time. The velocity profile for laminar flow in a circular tube is given by

$$u(r) = 2\langle V \rangle \left(1 - \frac{r^2}{R^2}\right) \tag{5.2}$$

where R is the tube radius and $\langle V \rangle$ is the area-averaged fluid velocity. Taylor derived an expression for the area-averaged concentration, $\langle c \rangle_{\text{area}}$ profile following a solute delta-pulse input for the case where axial convection dominates axial diffusion. The area-averaged concentration profile is proportional to a modified Gaussian profile,

$$\langle c \rangle_{area} \propto \frac{1}{\sqrt{t}} \exp\left(-\frac{\left(z - \langle V \rangle t\right)^2}{4D^* t}\right) \tag{5.3}$$

where D^* is an effective dispersion coefficient. Aris later demonstrated that the effective dispersion coefficient is given by

$$D^* = D + \frac{\langle V \rangle^2 R^2}{48D} \quad . \tag{5.4}$$

The dispersion is increased by velocity gradients with faster diffusers proving to be most capable of diminishing the velocity gradient induced dispersion.

The *Viscosizer*^{TM} *200* determines the solute dispersion coefficient and, ultimately the solute diffusion coefficient, by comparing the widths of the solute peak measured at two different times (or distances along the circular tube). Denoting the peak width as τ, the diffusion coefficient is calculated from

$$D = \frac{R^2(t_2 - t_1)}{24(\tau_2^2 - \tau_1^2)} \tag{5.5}$$

where 1 and 2 denote the first and second peak respectively, *t* denotes the peak arrival time [58]. It is assumed that

$$D^* \cong \frac{\langle V \rangle^2 R^2}{48D} \tag{5.6}$$

as first proposed by Taylor for the case wherein axial convection dominates axial diffusion. A moments analysis of equation (5.1) under the assumptions of Taylor yields a peak arrival time (first moment) given by $t_i = L_i/\langle V \rangle$ where L_i is the distance to the peak *i* detection window. The peak width (second moment) corresponding to this condition is given by $(\tau_i)^2 = 2D^*L_i/\langle V \rangle^3$.

5.3 Taylor Dispersion Measurements

5.3.1 Spreading of a Solute Delta-Pulse Input

Figure 5.1 illustrates solute plug flow through a capillary. When the sample front reaches detection window W1, absorbance increases to a maxima at highest concentration and soon drops down to the baseline once the plug passes the entire window yielding the area-averaged longitudinal concentration profile.

A similar phenomenon is observed at window W2, however the observed area-averaged concentration profile exhibits a larger width than is observed at W1. As noted previously, faster diffusing solutes yield smaller effective axial dispersion coefficients. Figure 5.2 displays the area-averaged concentration profiles observed at each window for BSA in dispersed in PBS at a 5mg/ml injection concentration. It is apparent that the peak detected at W2 is broader than the peak observed at W1 indicating that further dispersion has taken place in the intermittent time. The protein diffusion coefficient can be calculated from equation 5.5 by incorporating variance and absorbance peak times at W1 and W2.

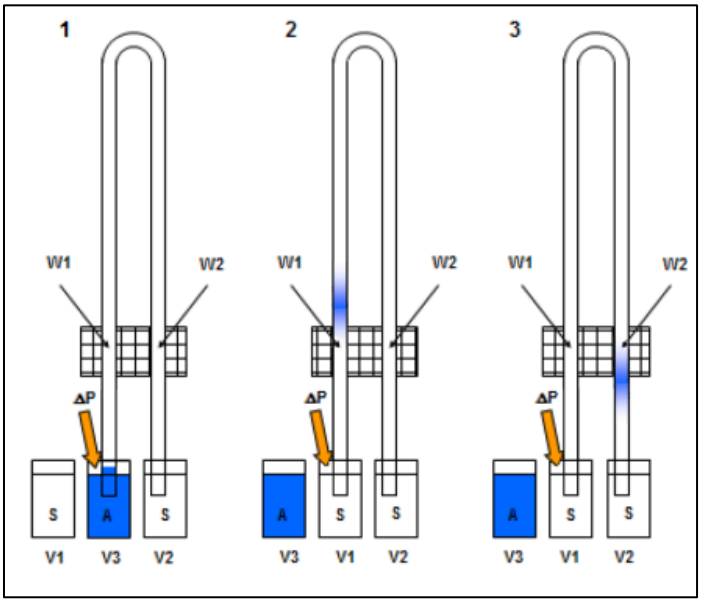

Figure 5.1 Injection of sample plug and flow across detection windows 1 and 2 *[58]*.

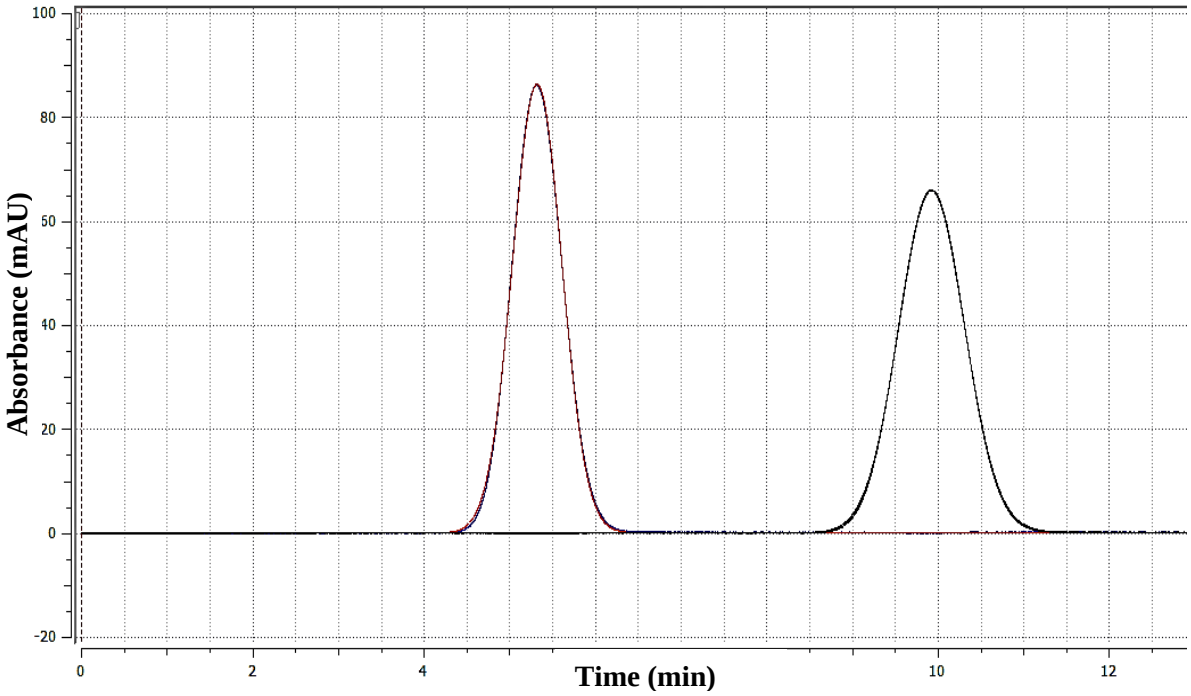

Figure 5.2 Taylor dispersion trace for an injection of 5mg/ml BSA dispersed in PBS.

5.3.2 Taylor Dispersion Analysis Determination of BSA Diffusion Coefficients

Representative BSA diffusion coefficients determined from Taylor dispersion analysis are presented as a function of BSA injection concentration in Figure 5.3. This case of BSA dissolved in 50 mM Tris was previously considered in Chapter 4 wherein dynamic light scattering measurements of the BSA diffusion coefficients are presented. While the focus is on TDA in Chapter 5, the DLS and TDA measurements are compared and discussed in Chapter 6. Here it will suffice to note the same qualitative behavior is observed. That is, the BSA collective diffusion coefficient is observed to increase with increasing BSA concentration as expected for this case of repulsive protein-protein interactions. The noisy low concentration data owes to the use of the 280 nm optical filter for entire measurement series with sensitivity being greatly diminished for concentrations less than 10 mg/ml (see

Figure 5.3). Though, for accurate measurements of concentrations below 10mg/ml a 214nm filter should be used (Section 5.2.4), here in order to show the overall trend of diffusion coefficient a 280nm filter was used for all concentrations.

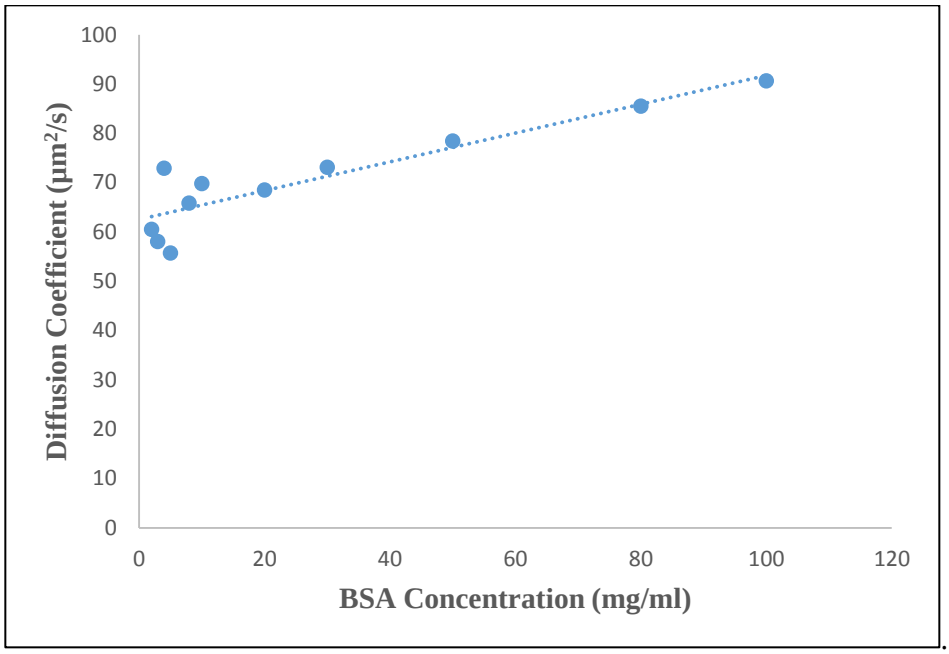

Figure 5.3 Diffusion coefficients measured for BSA dispersed in 50 mM Tris as a function of BSA injection concentration. The measurements were made with a 280nm filter.

5.3.3 Observation of Injection Concentration Dependent Peak Arrival Times

An interesting observation was made regarding the arrival time of peak 2. This effect is illustrated in Figure 5.4 where the area-averaged concentration profiles of BSA in PBS solutions of varying injection concentration are displayed. Focusing on detector window 2

(the second peak in Figure 5.4) it is readily apparent that the peak 2 arrival time increases as the BSA injection concentration is increased from 10 to 50 mg/ml.

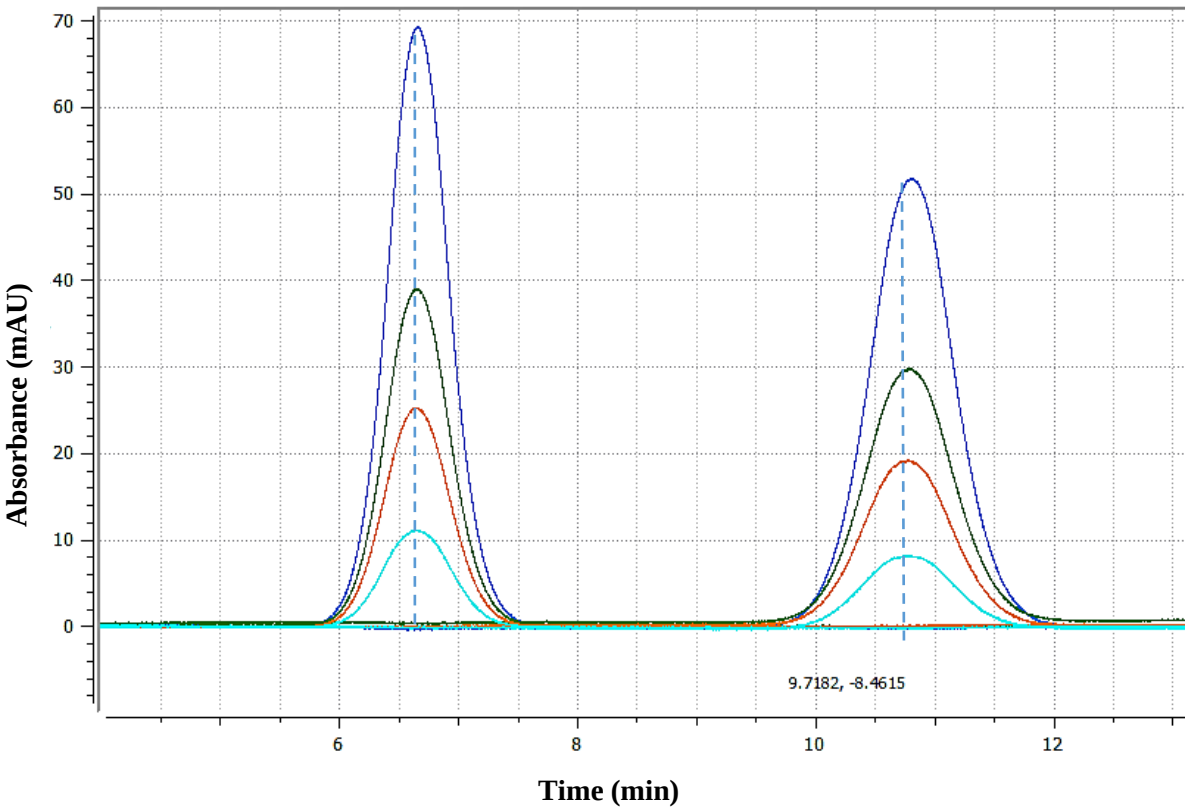

Figure 5.4 Taylor dispersion peaks observed for BSA dispersed in 50 mM Tris for BSA injection concentrations of 10, 20 30 and 50mg/ml. An increase in absorbance and an increase in the second peak arrival time are observed with increasing BSA concentration.

One primary assumption of Taylor's analysis is that the problem is quasi-steady such that the concentration profile should be translated with mean speed <*V*> [38]. This condition is obviously being violated in the measurements presented here since the peak 2 arrival time is not constant and actually increases with increasing BSA injection concentration. There is a very slight shift of peak arrival time shift to later times for the case of peak 1 as well.

In general the arrival time of the peak maximum is given by [59]

$$t = \frac{L}{\langle V \rangle}\left[1 + \frac{2D^*}{\langle V \rangle L}\right]. \tag{5.7}$$

for the case of a constant D^*. Consideration of this expression in relation to the observations of Figure 5.4 indicates the effective dispersion coefficient is increasing with increasing BSA injection concentration. An increasing dispersion coefficient is indicative of a decreasing BSA collective diffusion coefficient with increasing BSA concentration. However, the DLS measurements presented in Chapter 4 demonstrate the BSA collective diffusion coefficient will increase with increasing BSA concentration for BSA dispersed in 50 mM Tris – as expected for this case of repulsive protein-protein interactions. In addition, the second term in equation (5.7) is less than 1% of the first term when calculated with the appropriate physical constant values. Finally, the system under considerations is well within the geometric and Peclet number limits required by the Taylor-Aris solution to the constant diffusion coefficient convective diffusion equation. This indicates the observed delay in the peak 2 arrival time must result from some phenomenon not accounted for at the level of the Taylor-Aris approximation. The discrepancy most likely results from the collective diffusion coefficient concentration dependence altering the dispersion process in a manner that cannot be captured by the approximations inherent to the Taylor-Aris analysis.

The correct convective diffusion equation includes a concentration dependent collective diffusion coefficient, $D(c)$,

$$\frac{\partial c}{\partial t} + u(r)\frac{\partial c}{\partial z} = D(c)\frac{\partial^2 c}{\partial z^2} + \frac{1}{r}\frac{\partial}{\partial r}\left(rD(c)\frac{\partial c}{\partial r}\right) \tag{5.8}$$

This exact convective diffusion equation is a topic of current study within at BTEC. Assuming that the collective diffusion coefficient concentration dependence is described in the standard manner (equation 2.5), it is hoped that the protein interaction parameter k_D can be extracted from a single Taylor dispersion measurement.

5.3.4 Linear Light Absorption Concentration Range

Optical filters of different wavelengths (214, 254 and 280nm) are provided for *Viscosizer 200* from Malvern. When characterizing protein solutions the 214 nm filter is recommended for concentrations below 10 mg/ml with the 280 nm filter utilized for all higher concentrations. If the 280 nm filter is used for concentrations lower than 10mg/ml noisy, low signal concentration traces will result. In order to assess the suitability of this recommendation, TDA measurements of BSA in Tris 50mM pH 8.0 were performed using both 280 and 214 nm optical filters. In Figure 5.5 the measured light absorption is presented as a function of protein (BSA) concentrations up to and including 100 mg/ml.

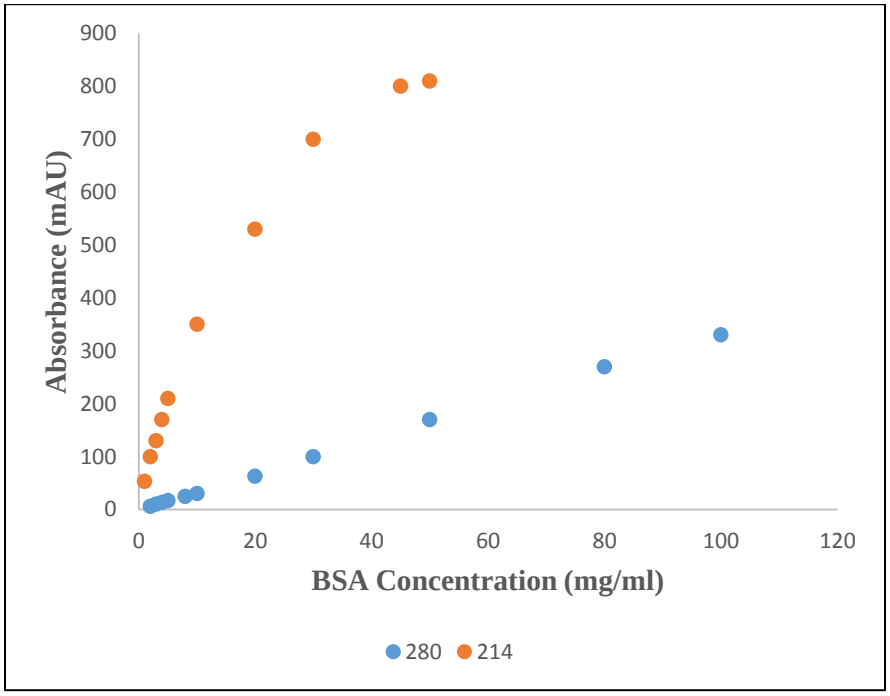

Figure 5.5 *Viscosizer 200* light absorbance measurements for BSA dispersed in 50 mM Tris using 214 and 280 nm optical filters.

Two observations are important. First, the 214 nm absorbance values become non-linear very quickly and it appears the protein concentrations ≤ 10 mg/ml recommendation is valid. Secondly, although the 280 nm absorption is linear across the entire concentration range considered here, the weak absorbance values observed for the low concentrations behooves the use of the 214 nm filter for this concentration range.

In order to demonstrate the potential errors that can result from an improper filter choice, TDA diffusion coefficient determinations were conducted with both optical filters for BSA solutions of varying injection concentrations. The optical filter choice influences the measured diffusion coefficient values to the point of obscuring the actual behavior. The resultant measurements are shown in Figure 5.6. DLS measurements unequivocally demonstrated that the collective diffusion coefficient of BSA dispersed in Tris increases with

increasing BSA concentration (Chapter 4). This expected trend is confirmed when the 280 nm filter is utilized in TDA measurements – albeit the low concentration data is very noisy. However, when the 214 nm filter is utilized the completely opposite trend is observed – the BSA collective diffusion coefficient decreases with increasing concentration. This discrepancy results from overestimating the half height peak width of absorbance. It has been qualitatively understood that overall peak absorbance is truncated because of a loss of sensitivity when using the 214 nm filter at high concentrations. This was related to the non-linearity shown in Figure 5.5. This leads to an overestimation of the dispersion coefficient, which in turn yields an *underestimated* diffusion coefficient. The optimal measurement method would utilize the 214 nm filter at low concentrations (≤ 10 mg/ml) and 280 nm at higher.

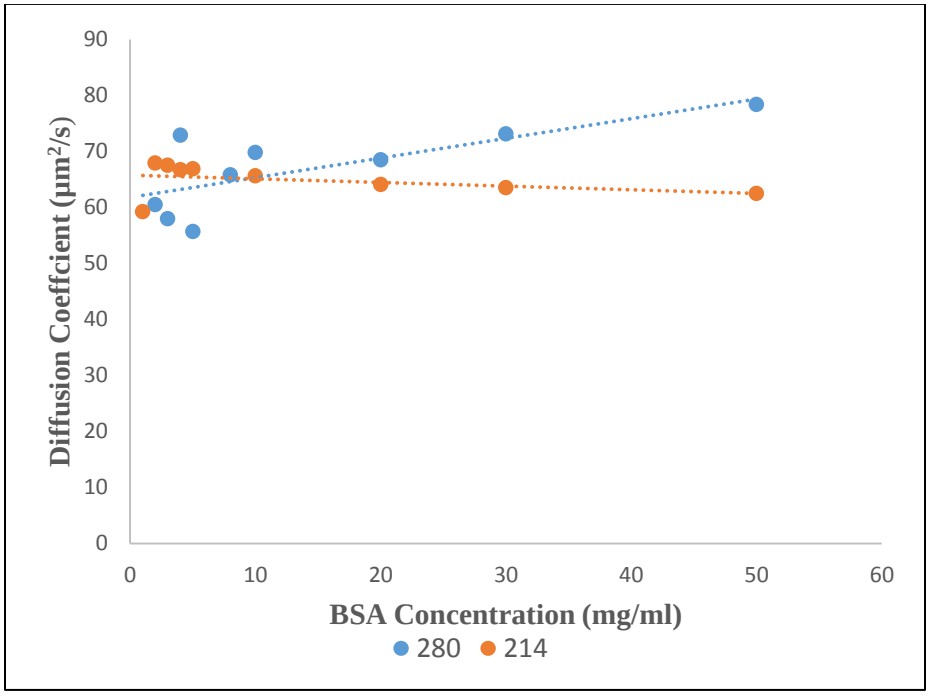

Figure 5.6 Diffusion coefficients for BSA in 50 mM Tris measured for the cases of 214 and 280 nm optical filters. Y-axis represents diffusion coefficient that starts to follow an opposite trend for 214 vs 280 with increase in concentration beyond 10mg/ml as seen in the above Figure.

5.4 Conclusions & Summary

This chapter outlined the basic principles of the Taylor dispersion analysis method for determining solute diffusion coefficients. TDA was capable of capturing the qualitative behavior of the protein collective diffusion coefficient concentration dependence given a proper choice of optical filter to ensure the dispersion peaks are properly measured. Deviations from the expected Taylor analysis behavior were observed for sufficiently concentrated protein solutions. It is proposed the observed deviations are a result of neglecting the protein collective diffusion coefficient concentration dependence as part of the Taylor analysis of the convective diffusion equation. As demonstrated in Chapter 4, the concentration effects on protein-protein interactions can be quite pronounced for the protein concentrations considered here.

Chapter 6

DLS and TDA Comparison

This chapter compares and contrasts protein collective diffusion coefficients measured by both dynamic light scattering and Taylor dispersion analysis. The measured values are considered qualitatively and quantitatively during the discussion. (See Appendix A for diffusion coefficient values)

6.1 Results & Discussion

Following the linear concentration range study performed for TDA (Chapter 5), measurements of concentrations ≤ 10mg/ml were conducted with a 214nm optical filter and a 280nm filter for higher than 10mg/ml. TDA and DLS measurements were carried out on the same day to minimize any sample aging effects. For data represented in this Chapter, BSA in Tris solution was filtered with 0.02 µm filters prior to measurement and BSA in PBS and Tris/1 M ammonium sulphate solutions were filtered using 0.1 µm filters. No significant difference was observed between filtration with 0.02 versus 0.1 µm filters based on FFF separation and absorbance.

There are several things to keep in mind when considering these data. First, the DLS data depicts the true collective diffusion coefficient value for a given protein concentration since this concentration value is fixed at all points within the sample volume. Secondly, the protein concentration reported for the TDA measurements is the *injection* concentration. Not only is the protein concentration diluted upon injection into the TDA analyzer, but the protein concentration varies in space and time throughout the measurements. This will have

some impact on the measured protein collective diffusion coefficient values as well as their concentration dependence as will be demonstrated here.

Figures 6.1-6.3 display the protein collective diffusion coefficients measured by DLS and TDA for BSA dispersed in 50 mM Tris, PBS and 50 mM Tris/1 M ammonium sulphate. While the qualitative agreement between data sets is quite good based on the trends observed for BSA diffusion coefficient with increase in concentration, fairly significant quantitative differences are observed (Table 6.1).

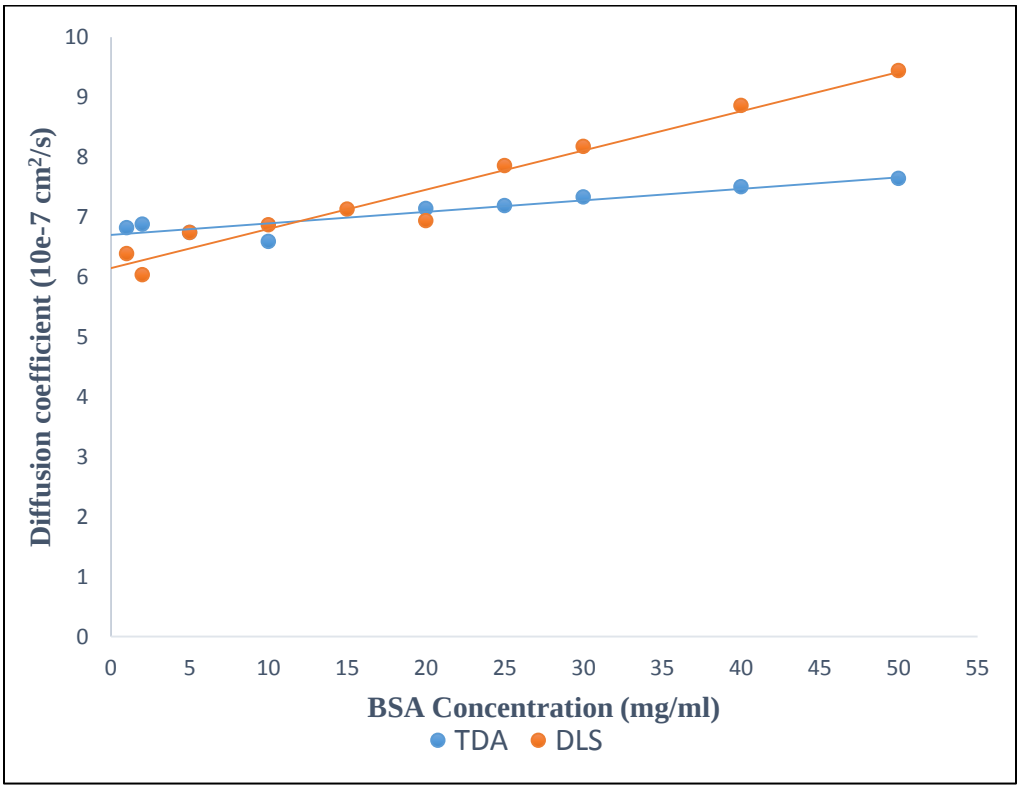

Figure 6.1 BSA diffusion coefficient in 50 mM Tris. Comparison of results from DLS and TDA.

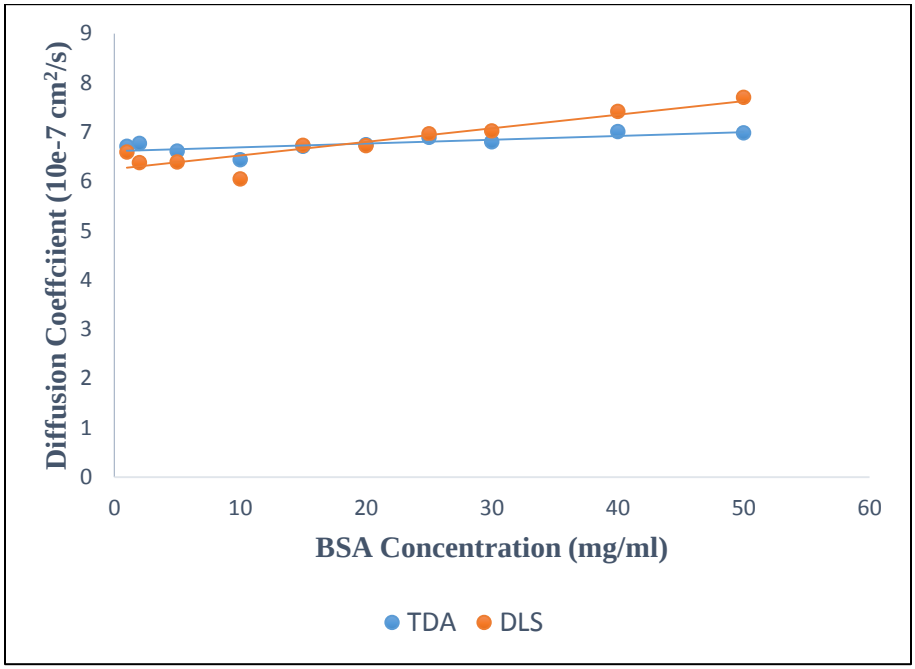

Figure 6.2 BSA diffusion coefficient in PBS. Comparison of results from DLS and TDA.

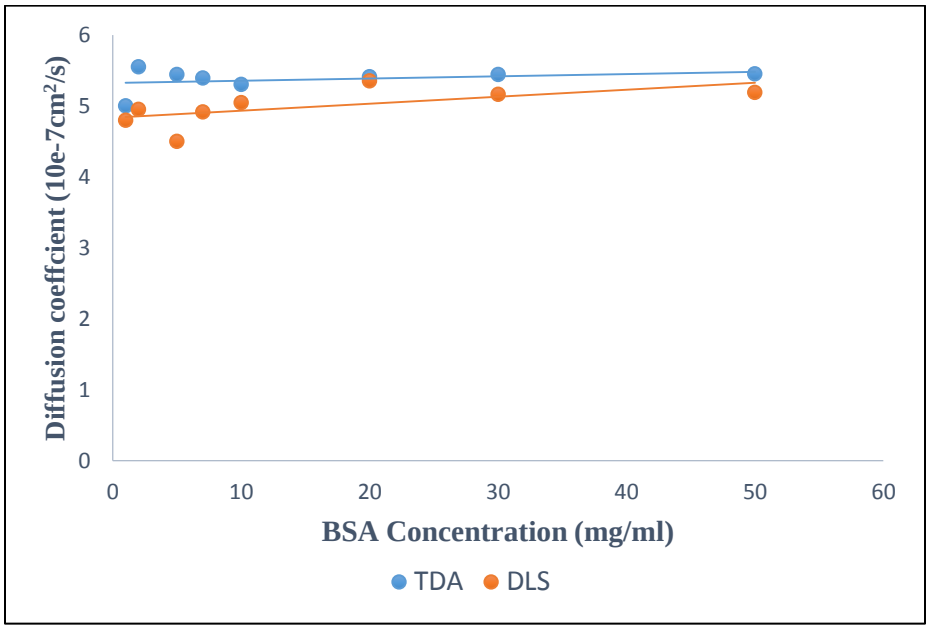

Figure 6.3 BSA diffusion coefficient in 50 mM Tris/1 M ammonium sulphate. Comparison of results from DLS and TDA.

The quantitative agreement between DLS and TDA at sufficiently low protein concentrations is quite good. Recall that the protein collective diffusion coefficient concentration dependence will not be very pronounced at low concentrations other than the case of very large magnitude k_D values. Quantitative, that is, diffusion coefficient value differences are most noticeable at the higher concentrations where the effects of protein-protein interactions take on greater importance. The most pronounced quantitative differences occur for BSA dispersed in 50 mM Tris. The disagreement here is a result of the relatively strong repulsive protein-protein interactions present in that system leading to a strong protein collective diffusion coefficient concentration dependence.

Quantitative differences diminish as the protein-protein interactions decrease as the buffer changes from 50 mM Tris to PBS. The difference in diffusion coefficient measurements of TDA and DLS was observed to be greater with increasing concentration as can be seen in Figures 6.1 and 6.2. BSA in Tris/1 M ammonium sulphate system exhibits very little protein-protein interactions understood qualitatively by looking at the slope (Figure 6.3) and quantitatively by much lower values of k_D (Table 6.1). This is indicated by the negligible protein collective diffusion concentration dependence observed for both DLS and TDA measurements.

Some of the observed discrepancies between DLS and TDA measurements at high concentrations result from the fact the presented protein concentrations for the TDA measurements are the protein injection concentrations. In actuality the protein concentration will be less than this value owing to dilution effects thereby decreasing the protein collective diffusion coefficient for the case of repulsive protein-protein interactions ($k_D > 0$). In addition to this fact, one must consider the manner in which TDA determines collective diffusion coefficients. While Taylor's original analysis assumed the collective diffusion coefficient was constant, the protein dispersions considered here will exhibit concentration dependent collective diffusion coefficients with these effects being most pronounced for the

large protein injection concentrations. The protein concentration will vary across the dispersion peak with lower concentration protein solutions exhibiting smaller collective diffusion coefficients than the large concentration regions. As such, the dispersion peak concentration profile will not be that described by Taylor in his original solution of the problem.

As noted in the previous chapter, the solution of the convective diffusion equation for this case is quite complex and is a subject of current study in the BTEC research group. However, the expected overall effect is a reduction in the collective diffusion coefficient values measured via TDA in comparison with those found from DLS measurements. This owes to the fact that the average protein collective diffusion coefficient in the TDA measurement is smaller than its peak value which in turn is still smaller yet than the value measured by DLS. The smaller slopes observed for the protein collective diffusion coefficient concentration dependence in Figures 6.1-6.3 confirm this expectation. The quantitative differences are shown in Table 6.1 where the determined protein interaction parameter, k_D, values are presented for the DLS and TDA methods. While the TDA method can capture the qualitative protein-protein interaction trend, it is apparent that the TDA significantly underestimates the strength of protein-protein interactions thereby preventing the use of traditional TDA analysis for characterizing protein-protein interactions in a quantitative manner.

TABLE 6.1 Interaction parameter (k_D) values from DLS and TDA.

Technique	**k_D values from different solvents (ml/g)**		
	50mM Tris	**PBS**	**50mM Tris/1M ammonium sulphate**
DLS	10.7	4.4	2.0
TDA	2.9	1.2	0.6
% decrease in k_D from DLS to TDA	72.89	72.72	70

Chapter 7

Conclusions & Future Work

7.1 Conclusion

Protein-protein interactions play a primary role in determining colloidal stability. DLS was confirmed as a robust method for characterizing protein-protein interactions albeit with some remaining ambiguities pertaining to the accessibility of fundamental interparticle interaction parameters such as the second osmotic virial coefficient via this method. TDA was considered for the first time ever as a tool for investigating protein-protein interactions. While TDA was demonstrated to *qualitatively* capture the correct protein-protein interaction behavior by giving similar trends to DLS, it was observed to fail *quantitatively* for strongly interacting protein concentrations at sufficiently high concentrations. This failure is believed to occur as a consequence of the assumptions inherent to current Taylor dispersion analysis approaches to data analysis. The primary constraining assumption is that of a *constant* protein collective diffusion coefficient. However, the DLS measurements presented herein demonstrate that the protein collective diffusion concentration dependence can be quite pronounced for many typically encountered protein solutions. Neglecting the protein collective diffusion coefficient concentration dependence will lead to an underestimation of the actual protein collective diffusion coefficient determined from TDA thereby underestimating the magnitude of protein-protein interactions.

7.2 Future Work

7.2.1 Taylor Dispersion Analysis

Work to date indicates the protein collective diffusion coefficient concentration dependence plays a significant role in Taylor dispersion analysis. As shown in Chapter 5, the convective diffusion equation is not amenable to standard Taylor-Aris analysis when a concentration dependent collective diffusion coefficient is considered. Current work in BTEC focuses on developing new analytic methods for tackling this modified convective diffusion equation in an attempt to develop a method that will allow for the determination of the protein interactions parameter, k_D, from a single dispersion measurement. If this research track succeeds it will prove highly beneficial as a high-throughput technique, compared to the traditional methods such as DLS, for characterizing protein-protein interactions and gain insight into protein dispersion colloidal stability.

7.2.2 Solidifying DLS-based Methods for Assessing Protein Colloidal Stability

Research at BTEC will also focus on utilizing simultaneous SLS and DLS experiments to assess the applicability of the Prinsen-Odijk theory of protein-protein interactions. This experimental approach will allow for the direct comparison of B_{22} and k_D and it is hoped it will provide a means for assessing B_{22} indirectly via DLS measurements. Future work will include the consideration of other proteins and buffer compositions with the objective of a very detailed study of ionic strength effects for several salts following the Hofmeister series.

REFERENCES

[1] S. M. Moe, Y. J. Wang and S. Hershenson, "The Structure of Biological Therapeutics," in *Formulation and Process Development Strategies for Manufacturing Biopharmaceuticals* , pp. 1-40.

[2] B. Leader , Q. J. Baca and D. E. Golan , Protein Therapeutics: a summary and pharmacological classification.

[3] D. Voet and J. G. Voet, Basic concepts of Protein Structure, Joyce J. Diwan , 2003.

[4] A. L. Lehninger, D. L. Nelson and M. M. Cox , Principles of BIochemistry, pg.171.

[5] C. Pace, B. Shirley , M. McNutt and K. Gajiwala , Forces Contributing to the Conformational Stability of Proteins, FASEB J, 1996 Jan .

[6] S. Paulo, *Braz J. Chem. Eng.* , vol. 17, pp. 4-7, Dec 2000.

[7] B. S. Chang, B. Yeung, F. Jameel and S. Hershenson, "Physical Stability of Protein Pharmaceuticals," in *Formulation and Process Development Strategies for Manufacturing Biopharmaceuticals* , John Wiley & Sons Inc, 2010.

[8] M. Hora, "Manufacturing Fundamentals for Biopharmaceuticals," in *Formulation and Process Development Startegies for Manufacturing Biopharmaceuticals* , John Wiley & Sons Inc, 2010.

[9] D. X. Shaoxin Li and J. Li, "Dynamic Light Scattering Application to Study Protein Interactions in Electrolyte Solutions," *Journal of Biological Physics* , pp. 313-324, 2004.

[10] R. Nayar and M. Mosharraf , "Effective Approches to Formulation Development of Biopharmaceuticals," in *Formulation and Process Development Strategies for Manufacturing Biopharmaceuticals* , John Wiley & Sons, Inc , 2010.

[11] "Ligth Scattering for the Masses - Thermal Stability as a Function of pH and Concentration," Wyatt Technology corporation, 2012.

[12] J. R. Alford, B. S. Kendrick , J. F. Carpenter and T. W. Randolph, "Measurement of the Second Osmotic Virial Coefficient for Protein Solutions exhibiting monomer-dimer equilibrium," *Anal Biochem* , pp. 128-33, 2008 Jun.

[13] K. A. Majorek, P. J. Porebski , A. Dayal , M. D. Zimmerman, K. Jablonska, A. J. Stewart, M. Chruszcz and W. Minor , "Structural and Immunologic Characterization of Bovine Horse, and Rabbit Serum Albumins," *Mol. Immunol,* no. PubMed: 22677715 PubMedCentral: PMC3401331, pp. 174-182, 2012.

[14] S. Ge, K. Kojio, A. Takahara and T. Kajiyama, "Bovine Serum Albumin Adsorption onto Immobilized Organotrichlorosilane Surface: Influence of the Phase Separation on Protien Adsorption Patterns," *Biomater Sci Polym Ed,* pp. 131-50, 1998.

[15] S. Amin , G. V. Barnett, J. A. Pathak, C. J. Roberts and P. S. Sarangapani, "Protein Aggregation, Particle Formation, Characterzation & Rheology," *Current Opinion in Colloid & Interface Science,* vol. 19, no. 5, pp. 438-449, 2014.

[16] L. Munishkina, E. Cooper, V. Uversky and A. Fink , "The Effect of Macromolecular Crowding on Protein Aggregation and Amyloid Fibril Formation," *Mol Recognit,* pp. 456-64, 2004.

[17] A. Horwich, "Protein Aggregation in Disease: A Role for folding Intermediates Formin Specific Multimeric Interactions," *Clinical investigation J,* pp. 1221-1232, 2002 Nov.

[18] B. D. e. a. Connolly, "Weak Interactions Govern the Viscosity of Concentrated Antibody Solutions: High-Throughput Analysis Using Diffusion Interaction Parameter," *Biophys J,* vol. 103, no. 1, pp. 69-78, July 2012.

[19] "Module 8: Lecture 37: Stability of Colloids," [Online]. Available: http://nptel.ac.in/courses/103104045/pdf_version/lecture37.pdf.

[20] J. Israelachvili , Intermolecular and Surface Forces, 3 ed, Academic Press London, 2011.

[21] J. Israelachvili and R. M. Pashley, *J. Colloid Interface Sci*, 1984.

[22] Y. Zhang , E. Farrell, D. Mankiewicz and Z. Weiner, "Brookhaven Instruments Corporation," [Online]. Available: http://www.brookhaveninstruments.com/literature/library/study-of-protein-hydrodynamics-with-light-scattering-size-and-charge-of-lysozyme.

[23] H. Hwang , "Final Project for AP225 Fall 2011," [Online]. Available: http://soft-matter.seas.harvard.edu/index.php/DLVO_theory.

[24] *Langmuir* , 2005.

[25] B. L. Neal , D. Asthagiri, O. D. Velev, A. M. Lenhoff and E. W. Kaler, "Why is the Osmotic Second Virial Coefficient Related to Protein Crystallization," *Journal of Crystal Growth*, pp. 377-387, 1999.

[26] E. R. Lima, F. W. Tavares and E. C. Biscaia Jr, Ion-Specific Potential of Mean Force Between two Aqueous Proteins, Elsevier B.V./Ltd, 2008.

[27] J. v. Zanten, *Biological Processing Science BEC 532*, BTEC, North Carolina State University, 2013.

[28] W. G. McMillan and J. E. Mayer, *J.Chem.Phys.* , no. 13, p. 276, 1945.

[29] A. Saluja, R. M. Fesinmeyer, S. Hogan, D. N. Berms and Y. R. Gokarn, "Diffusion and Sedimentation Interaction Parameters for Measuring the SEcond Virial Coefficient and Their Utility as Predictors of Protein Aggregation," *Biophys J*, pp. 2657-2665, 2010.

[30] H. Vink, *J.Chem. Soc. Farad Trans*, 1985.

[31] P. Prinsen and T. Odijk, "Collective diffusion coefficient of proteins with hydrodynamic, electrostatic and adhesive interactions," *J Chem Phys*, vol. 127, no. 11, 2007 Sep .

[32] C. Lehermayr, H. C. Mahler, K. Mader and S. Fischer, *Journal of Pharmaceutical Sciences* , pp. 2551-2562, 2011.

[33] R. L. Baldwin, "How Hofmeister ion interaction affect protein stability," *Biophysical Journal* , vol. 71, pp. 2056-2063, 1996 Oct.

[34] F. Hofmeister, "Zur Lehre von der Wirkung der Salze," *Arch. Exp. Pathol. Pharmakol*, pp. 247-260, 1888.

[35] W. Kunz, J. Henle and B. W. Ninham, "Zur Lehre von der Wirkung der Salze' (about the sciencew of the effect of salts: Franz Hofmeister's historical papers," *Curr. Opin. Colloid Interface Sci.* , vol. 9, pp. 19-37, 2004.

[36] M. Bostrom , D. F. Parsons, A. Salis, B. W. Ninham and M. Monduzzi, "Possible Origin of the Inverse and Direct Hofmeister Series for Lysoyme at Low and High Salt Concentrations," *Langmuir*, vol. 27, no. 15, pp. 9504-9511, 2011.

[37] Y. Zhang and P. S. Cremer, "Interactions between Macromolecules and Ions: The Hofmeister series," *Current Opinion in Chemical Biology* , vol. 10, no. 6, pp. 658-663, 2006 Dec.

[38] S. G. Taylor, "Dispersion of soluble matter in solvent flowing through a tube," Mar 1953.

[39] "Asymmetrical Flow Field-Flow Fractionation Fraunhofer Institute for Industrial Mathematics," [Online]. Available: http://www.itwm.fraunhofer.de/en/departments/flow-and-material-simulation/hydrodynamics/asymmetrical-flow-field-flow-fractionation.html.

[40] "Eclipse AF4: The ultimate system for separating macromolecules, proteins, colloids and nanoparticles.," Wyatt Technology , [Online]. Available: http://www.wyatt.eu/index.php?id=eclipse.

[41] H. B. Bohidar, "Light Scattering Study of Solution Properties of Bovine Serum Albumin, Insulin and Polystyrene under Moderate Pressure," *Colloid and Polymer Science*, vol. 267, no. 4, 1989.

[42] D. Arzensek, "Dynamic Light Scattering and Application to Proteins in Solutions," University of Ljubljana, 2010 May.

[43] "Dynamic Light Scattering: Measuring the Particle Size Distribution," LS Instruments , [Online]. Available: http://www.lsinstruments.ch/technology/dynamic_light_scattering_dls/.

[44] P. Morters and Y. Peres, "Brownian Motion," 2008. [Online]. Available: http://research.microsoft.com/en-us/um/people/peres/brbook.pdf.

[45] A. Einstein , Inestigations on the Theory of the Brownian Movement, Dover Publication Inc, 1926.

[46] "Static light scattering vs. Dynamic light scattering," [Online]. Available: http://www.chem.iitkgp.ernet.in/faculty/SDG/Scattering%20by%20macromoleculesII.pdf.

[47] "Understanding Dynamic Light Scattering," Wyatt Technology , [Online]. Available: http://www.wyatt.com/theory/theory/understanding-qels-dynamic-light-scattering.html.

[48] B. Chu , Laser Light Scattering: Basic Principles and Practice, Boston : Academic Press, 1991.

[49] R. Pecora and B. J. Berne, Dynamic Light Scattering: With Application to Chemistry, Biology and Physics., Dover Publications, third edition, 2000.

[50] S. J. Walker, "The Stokes-Einstein Law for Diffusion in Solution," *Proceesings of the Royal Society of London* , vol. 106, 1924 Dec.

[51] D. E. Koppel, "Analysis of macromolecular polydispersity in intensity correlation spectroscopy: The method of cumulants.," *The Journal of Chemical Physics,* vol. 57, no. 11, Dec 1972.

[52] ASTRA 6.1 guide, Wyatt Technology .

[53] "Concentration properties of aqueous solutions: Density, Refractive Index, Freeezing point

Depression and Viscosity," [Online]. Available: http://chemistry.mdma.ch/hiveboard/rhodium/pdf/chemical-data/prop_aq.pdf.

[54] Y. Zhang and P. S. Cremer , "The Inverse and Direct Hofmeister Series for Lysozyme," *PNAS*, June 2009.

[55] R. Aris, "On the dispersion of a solute in a fluid flowing through a tube," Sep 1955. [Online]. Available: http://rspa.royalsocietypublishing.org/. [Accessed 30 Nov 2014].

[56] A. Hawe, W. L. Hulse, W. Jiskoot and R. T. Forbes, "Taylor Dispersion Analysis Compared to Dynamic Light Scattering for the Size Analysis of Therapeutic Peptides and Proteins and Their Aggregates," *Pharma Res*, vol. 28, pp. 2302-2310, 2011.

[57] Stewart, Lightfoot & Bird, Transport Phenomena, 2002.

[58] Viscosizer 200 Manual, Malvern Intruments , 2013.

[59] E. Grushka, Chromatographic Peak Shapes. Their Origin and Dependence on the Experimental Parameters, Buffalo, New York : Department of Chemistry, State University of New York at Buffalo, Feb 1972.

APPENDIX

APPENDIX A – Diffusion Coefficient Values

The Viscosizer (TDA) reports diffusion coefficient in μm^2/sec and these values were converted to cm^2/sec.
For DLS measurements, the diffusion coefficient was calculated by applying Stokes-Einstein relation

$$D_0 = \frac{k_B T}{6\pi\eta R_H}$$

D_0 is the diffusion coefficient
Boltzmann's constant k_B = 1.38 x 10e-16 g cm^2 s^{-2} K^{-1}
Temperature, T = 298.25 K
Viscosity, η = 0.8892 cp
Hydrodynamic Radius, R_H, is the average radius obtained from regularization data.

Dynamic light scattering data – Diffusion coefficient (10e-7 cm^2/s) values for BSA

BSA Concentration (mg/ml)	50mM Tris	PBS	1M Amm S	2M Amm S
1	6.00	6.39	4.83	3.89
2	6.04	6.39	4.98	3.86
3	5.58	6.04	4.75	**
4	N/A	N/A	4.70	3.88
5	6.80	6.24	4.79	3.90
6	N/A	N/A	N/A	3.68
7	N/A	N/A	N/A	3.47
8	N/A	N/A	N/A	3.81
9	N/A	N/A	N/A	3.73
10	6.80	6.25	4.95	3.88
15	7.20	6.36	4.88	N/A
20	7.67	6.73	4.92	N/A
30	8.29	6.97	5.06	N/A
40	8.90	7.23	5.24	N/A
50	9.66	7.36	5.16	N/A

BSA Concentration (mg/ml)	50mM Tris	0.1 M Amm S	0.2 M Amm S	0.5 M Amm S	1 M Amm S	2 M Amm S
1	6.00	5.80	5.65	4.93	4.83	3.89
2	6.04	5.92	5.67	5.09	4.98	3.86
3	5.58	6.00	5.71	5.03	4.75	**
4	N/A	N/A	N/A	N/A	4.70	3.88
5	6.80	5.95	5.85	5.04	4.79	3.90
6	N/A	N/A	N/A	N/A	N/A	3.68
7	N/A	N/A	N/A	N/A	N/A	3.47
8	N/A	N/A	N/A	N/A	N/A	3.81
9	N/A	N/A	N/A	N/A	N/A	3.73
10	6.80	6.05	5.82	5.02	4.95	3.88
15	7.20	6.35	6.15	5.25	4.88	N/A
20	7.67	6.39	6.09	5.12	4.92	N/A
30	8.29	6.71	6.32	5.44	5.06	N/A
40	8.90	6.98	6.45	5.44	5.24	N/A
50	9.66	7.11	6.51	N/A	5.16	N/A

BSA Concentration (mg/ml)	1 M NaBr	1M NaCl	1M Amm S
1	5.62	5.13	4.83
2	5.58	5.29	4.98
3	5.57	5.45	4.75
5	5.70	5.53	4.79
10	5.82	5.51	4.95
15	5.86	5.70	4.88
20	5.89	5.77	4.92
30	6.26	5.71	5.06
40	6.33	5.95	5.24
50	6.42	6.10	5.16

TDA and DLS experiments

1. BSA in 50mM Tris

BSA Concentration (mg/ml)	**Diffusion coefficient from TDA (10e-7 cm^2/s)**	**Diffusion coefficient from DLS (10e-7 cm^2/s)**
1	6.82	6.38
2	6.88	6.03
5	6.74	6.74
10	6.59	6.87
15	**	7.13
20	7.14	6.94
25	7.19	7.85
30	7.33	8.17
40	7.50	8.86
50	7.64	9.44

2. BSA in PBS

BSA Concentration (mg/ml)	**Diffusion coefficient from TDA (10e-7 cm^2/s)**	**Diffusion coefficient DLS (10e-7 cm^2/s)**
1	6.71	6.59
2	6.77	6.38
5	6.61	6.39
10	6.44	6.05
15	6.71	6.73
20	6.74	6.73
25	6.89	6.96
30	6.80	7.02
40	7.01	7.41
50	6.98	7.70

3. BSA in 50mM Tris/1M ammonium sulphate

BSA Concentration (mg/ml)	**Diffusion coefficient from TDA (10e-7 cm^2/s)**	**Diffusion coefficient from DLS (10e-7 cm^2/s)**
1	5.00	4.80
2	5.55	4.95
5	5.44	4.50
7	5.39	4.91
10	5.30	5.04
20	5.41	5.35
30	5.44	5.16
50	5.45	5.19

N/A – Measurements were not carried out at these concentrations.
** - Measurement value was not included.